

Electronic Thesis and Dissertation Repository

6-19-2020 10:00 AM

Atypical Structural Connectivity and Integrity in Children with Hydrocephalus and its Relation to Executive Function

Daamoon Ghahari, *The University of Western Ontario*

Supervisor: Morton, J. Bruce, *The University of Western Ontario*

Co-Supervisor: de Ribaupierre, Sandrine, *The University of Western Ontario*

A thesis submitted in partial fulfillment of the requirements for the Master of Science degree in Neuroscience

© Daamoon Ghahari 2020

Follow this and additional works at: <https://ir.lib.uwo.ca/etd>



Part of the [Congenital, Hereditary, and Neonatal Diseases and Abnormalities Commons](#)

Recommended Citation

Ghahari, Daamoon, "Atypical Structural Connectivity and Integrity in Children with Hydrocephalus and its Relation to Executive Function" (2020). *Electronic Thesis and Dissertation Repository*. 7036.
<https://ir.lib.uwo.ca/etd/7036>

This Dissertation/Thesis is brought to you for free and open access by Scholarship@Western. It has been accepted for inclusion in Electronic Thesis and Dissertation Repository by an authorized administrator of Scholarship@Western. For more information, please contact wlsadmin@uwo.ca.

Abstract

Infants with hydrocephalus are a high-risk group for adverse neurodevelopmental outcomes, including impairments in executive functions such as goal-directed behaviour, focusing, and shifting attention. The current pilot study aimed to profile white matter and executive dysfunction in school-aged children with ventriculoperitoneal (VP) shunted hydrocephalus and age-matched healthy controls using the Behaviour Rating Inventory for Executive Functions and diffusion tensor imaging. To assess the degree of similarity between patient structural networks and controls, probabilistic streamlines between striatal and cortical regions and their respective diffusivity metrics were assessed. For a number of patients with hydrocephalus, white matter in the striatal-executive network showed significant deviation from a healthy control profile. Patients with higher global executive dysfunction also had lower correlations of striatal-executive fractional anisotropy with the healthy control profile. Future studies with larger samples can explore factors such as etiology that are likely to contribute to aberrant white matter and executive dysfunction.

Keywords

pediatric hydrocephalus, executive function, white matter integrity, structural connectivity, DTI

Summary for Lay Audience

Hydrocephalus is a neurological condition characterized by an abnormal accumulation of cerebrospinal fluid within the ventricles of the brain and is the most common reason for brain surgery in children. Infants with hydrocephalus are a high-risk group for adverse neurodevelopmental outcomes, including impairments in executive functioning (EF) skills such as goal-directed behaviour, focusing, and shifting attention. The current pilot study aimed to profile white matter integrity and executive dysfunction in school-aged children with ventriculoperitoneal (VP) shunted hydrocephalus and age-matched healthy controls using parental reports on the Behaviour Rating Inventory for Executive Functions (BRIEF2), and diffusion tensor imaging, a non-invasive MRI technique used to assess white matter microstructure *in vivo*. To assess the degree of similarity between patient and control structural networks, probabilistic streamlines between striatal and cortical regions of interest and their respective diffusivity metrics were assessed in native diffusion space. For a number of patients with hydrocephalus, white matter connectivity and diffusivity measured by fractional anisotropy (FA), mean diffusivity (MD), axial diffusivity (AD), radial diffusivity (RD) and magnetization transfer ratio (MTR) in the striatal-executive network showed significant deviation from a healthy control profile. Overall, patients with hydrocephalus displayed variable executive dysfunction outcome, with at least 5 patients scoring from the potentially clinically elevated to clinically elevated range across indices and another 2 patients scoring within the expected range for children of their age and gender. Patients with higher reported dysfunction on the Global Executive Composite (GEC) scale also had lower correlations of striatal-executive FA with the healthy control profile. Future studies with larger patient samples will be needed to explore factors such as etiology that are likely to contribute to aberrant white matter structure and executive dysfunction outcome.

Acknowledgments

I would like to thank my co-supervisors Dr. J. Bruce Morton and Dr. Sandrine de Ribaupierre for their endless support, guidance and collaborations that were vital in bringing this dissertation to life. Thank you for your time and dedication to your students' success, for your enthusiasm and understanding of the difficulties inherent in small-sample research. Thank you for letting me observe in the pediatric neurosurgery clinic and for all your scientific teachings. I would also like to thank all my advisors including Dr. A. Khan, Dr. R. Eagleson, and Dr. D. Mitchell for all their guidance and intellectual insights throughout my degree. I would like to thank our lab manager, Ms. Bea Goffin, for helping with our study's recruitment, mock scans and access to testing rooms. Thank you to the Centre for Functional and Metabolic Mapping staff, and specifically Scott Charlton, for helping us run our MRI scanning protocol, entertain our participants and parents and also troubleshoot our errors.

To all my lab members in the Cognitive Development and Neuroimaging Lab and 3DBrainViz Lab, and other colleagues in the WIRB, thank you for the mentorship, comradery, laughs, and both the hardships and good times we shared and endured. Every one of you taught me an important lesson throughout our time together. Thank you Ikhlas Hashi, for your support and for showing me the ropes at the beginning of my degree, starting with participant recruitment to running the study and neuroimaging protocol. I would also like to thank our volunteer Joud Hassoun for helping with recruitment and behavioural testing.

I would like to extend a special thank you to my partner, Gabriel do Valle, who was my rock and enduring support throughout the rollercoaster of graduate school. Thank you for pushing me to grow and believing in my dreams. Thank you to my family and friends, and also the families and participants who were a part of our study, without which this research would not be possible.

Finally, I would like to thank our funding sources: BrainsCAN and Children's Health Research Institute, for making this project possible. This research also benefited from the OurBrainsCAN registry that was funded by the Canada First Research Excellence Fund awarded to BrainsCAN at Western University.

Table of Contents

Abstract.....	ii
Summary for Lay Audience.....	iii
Acknowledgments	iv
Table of Contents.....	v
List of Tables	viii
List of Figures.....	ix
List of Appendices	xiii
Chapter 1	1
1 Introduction.....	1
1.1 Pathophysiology.....	1
1.2 Clinical Presentation & Symptoms.....	4
1.3 Shunt Treatment.....	5
1.4 Impacts on White Matter	6
1.5 Neurocognitive Outcomes Related to White Matter.....	7
1.6 Executive Functions.....	8
1.7 Diffusion Tensor Imaging.....	10
1.8 Magnetization Transfer Imaging.....	11
1.9 Current Study	11
Chapter 2.....	14
2 Methods.....	14
2.1 Participants.....	14
2.2 Patients with Hydrocephalus.....	14
2.3 Control Group.....	16
2.4 Socioeconomic Status	16

2.5 Behaviour Rating Inventory of Executive Functions.....	16
2.6 Neuroimaging Protocol.....	18
2.7 Structural & Diffusion MRI Acquisition & Parameters	19
2.8 Image Preprocessing.....	20
2.9 Tensor Estimation.....	20
2.10MTR estimation	22
2.11Harvard-Oxford Cortical FSL Atlas	23
2.12Oxford-GSK-Imanova Striatal Connectivity FSL Atlas.....	24
2.13Probabilistic Tractography.....	24
2.14Patient Shunts	26
2.15Isolating Sub-Striatal Networks.....	28
2.16Statistical Analysis.....	28
2.17Bootstrapped Correlation Distribution.....	29
2.18FA Linear Regression with GEC Scores	29
Chapter 3.....	32
3 Results.....	32
3.1 Behaviour Rating Inventory of Executive Functions.....	32
3.2 Striatal-Cortical Structural Connectivity	34
3.3 Striatal-Executive Network White Matter Integrity	34
3.4 FA Linear Regression with GEC	39
Chapter 4.....	43
4 Discussion	43
4.1 Executive Dysfunction.....	43
4.2 The Striatal Executive Network.....	45
4.3 Caveats & Limitations	49
4.4 Conclusions.....	50

References	52
Curriculum Vitae	67

List of Tables

Table 1. A list of all patients recruited for the study, with patients who were able to complete the diffusion neuroimaging protocol denoted with an asterisk (*). LBW= low birth weight, VLBW= very low birth weight, XLBW=extra low birth weight, IVH = Intraventricular Hemorrhage, DWM= Dandy-Walker’s Malformation, MG= meningitis, SB= Spina Bifida, and VP= ventriculoperitoneal.....15

Table 2. Interpretation of age and gender-standardized *t*-scores was based on the following guidelines obtained from the BRIEF2 scoring manual. A *t*-score of 50 represented the mean score of the normative population, with increasing scores representing higher degrees of executive dysfunction.....18

List of Figures

Figure 1. A schematic representation of CSF accumulation in the ventricular system of the brain in children with hydrocephalus. Typically, CSF which is continually produced in the ventricles flows back into systemic circulation and play several important roles for a healthy nervous system. When CSF flow is obstructed, intracranial pressure increases and the ventricular system can undergo rapid dilatation, severely impacting cortical and subcortical brain regions as well as periventricular white matter (From: Hydrocephalus, 2020)..... 3

Figure 2. Schematic representation of the clinical scales and respective composites scores measured by parental reports on the Behaviour Rating Inventory of Executive Function (BRIEF2). For the current study, the three composite scores (Behaviour Regulation Index, Emotion Regulation Index, and Cognitive Regulation Index) as well as the Global Executive Composite score was investigated in patients and controls. 17

Figure 3. Schematic of the diffusion tensor model calculated within each voxel of diffusion weighted volumes. Fractional anisotropy is a scalar value calculated as the square root of the sum of squares (SRSS) of the diffusivity differences, divided by the SRSS of the diffusivities. FA values closer to 1 represent higher white matter integrity. Mean diffusivity is calculated as the average of all three eigenvalues in mm^2/s . Axial diffusivity represents the principal diffusion vector, and is equal to the first eigenvalue in mm^2/s . Radial diffusivity represents diffusion perpendicular to the largest eigenvalue, and is calculated as the average of the second and third diffusivity eigenvalue in mm^2/s 21

Figure 4. Principal diffusivity vector maps modulated by fractional anisotropy were viewed for each subject during pre-processing to ensure correct tensor estimation before tractography. Higher FA is shown in yellow-green and the principal diffusivity vector (ϵ_1) is shown within each voxel. Correct tensor estimation was determined by examining the corpus callosum (as seen in the bottom-most panel) on a coronal slice.....22

Figure 5. Mask image of the 48 regions of interest (ROIs) from the Harvard Oxford Cortical Atlas and the 7 sub-cortical ROIs obtained from the Oxford-GSK-Imanova Striatal Connectivity FSL Atlas before non-linear transformation into native diffusion space (A).

Results of warping the ROIs into native diffusion space for patient 4A (B) and patient 5A (C).....24

Figure 6. Output of whole-brain probabilistic tractography for patient 5A, where voxels are coloured according to their raw streamline density. Blue voxels represent low streamline density whereas red represent high streamline density. Preliminary visual inspection of tractography revealed streamlines generated in line with the patient’s CSF shunt, highlighted with the arrow in coronal, sagittal, and axial slices (A). Manual segmentation of the patient’s shunt using an overlay on the T1-weighted image was then used to create a binary mask (green outline), which was dilated by 2-mm before transforming into diffusion space. This mask was then used as input to stop tracking streamlines if they entered this location (B). Manual shunt segmentations were performed for every patient.....27

Figure 7. Schematic representation of the bootstrap correlation procedure for control subjects. First, a single control subject is selected and removed from the control group pool (A). The extracted white matter metrics across tracts of interest for this single control subject, represented as “c” are then correlated with the mean profile of a bootstrapped sample of size n , represented as “b” and a single correlation coefficient is obtained. This process is iteratively repeated 10,000 for each control, each time randomly selecting from the control pool with replacement in order to obtain a different control mean profile and r value (C). Note that the control “c” is never included in the bootstrapped mean profile “b” as they were first excluded from the control pool to reduce inflation of the correlation co-efficient. Once all controls in the group have been bootstrapped, a histogram of the 190,000 computed correlation coefficients is constructed (D) and used to assess the probability of each patient’s correlation with the entire control group mean profile (E,F).....30

Figure 8. Age and gender standardized composite T scores of parental ratings on the Behaviour Rating Inventory for Executive Functions (BRIEF2). Patients with hydrocephalus are denoted with the letter ‘A ’and the mean t -scores for the control group are plotted with one SD . T -scores around 50 are indicative of average ratings for that age and gender. T -scores from 60 – 64 represent scores between 1 and 1.5 standard deviations above the mean, indicating mild executive dysfunction. T -scores from 65 – 69 represent scores between 1.5 and 2.0 standard deviations above the mean, indicating potentially clinical executive

dysfunction. A *t*-score of 70 or above represents 2 standard deviations above the mean, which indicates clinical executive dysfunction. Parental reports for Patient 4A displayed average *t*-scores around the mean, except on the Emotion Regulation Index, which indicates mild elevation. Parental reports for patient 5A demonstrated mild elevation of scores on both the Emotion Regulation Index and the Global Executive Composite. Patients 6A, 7A and 8A scored in the clinically elevated range on the Global Executive Composite and patient 10A on the Cognitive Regulation Index. The control group mean was within 1 *SD* of the age and gender standardized mean for neurotypically developing children.....33

Figure 9. (A) A symmetrical 55x55 structural connectivity matrix containing ROI-size corrected streamline counts, averaged across all controls and patients in the study. The color map represents the value of the connectivity index, with darker blues reflecting lower structural connectivity and yellows reflecting higher structural connectivity. The highlighted yellow column/row represents the tracts in the Striatum Executive network used for analysis. B) A structural connectivity vector of corrected streamline counts, containing tracts between the striatum executive sub-region and 21 cortical targets passing a weight-based threshold. The mean profile across healthy controls (*n*=19) is displayed in green with 95% confidence intervals and individual patients with hydrocephalus (*n*=7) are displayed in blue.....35

Figure 10. (A) The average fractional anisotropy (FA) in tracts seeded from the executive sub-region of the striatum is plotted for individual patients (*n*=7) in blue, and the control group mean profile is represented in green with 95% confidence intervals (*n*=19). The same visualization approach was used to assess (B) mean diffusivity (MD); (C) axial diffusivity (AD); (D) radial diffusivity (RD); and (E) the magnetization transfer ratio (MTR). There were less controls (*n*= 11) and patients (*n*=3) that were able to complete the MTR protocol as it was at the end of an hour-long imaging protocol.....38

Figure 11. (A) Control fractional anisotropy (FA) profiles across the striatal-executive network, were bootstrap correlated with randomly sampled control group mean profiles to obtain a distribution of correlation coefficients (10,000 correlations computed for each control; green). Patient fractional anisotropy (FA) profiles were correlated with the control group mean profile and plotted within the bootstrapped distribution (blue). Asterisks (*)

denote patients falling outside of the control bootstrap distribution with $p < .01$. The same steps were taken for profiles of MD (B), AD (C), RD (D) and MTR (E).....40

Figure 12. (A) A negative linear relationship was found between FA-correlations with the control mean profile in the striatal-executive network and the Global Executive Composite (GEC) scores across patients with hydrocephalus ($R^2=.728$, $F_{1,4}= 10.7$, $p<.05$). (B) FA-correlations of the striatal-occipital network were not able to significantly explain variability in the same GEC scores across patients ($R^2=.097$, $F_{1,4}= 0.431$, $p=.547$).....41

List of Appendices

Appendix A: Research Ethics Board Approval	65
Appendix B: Thresholding Striatal Networks.....	66

Chapter 1

1 Introduction

Hydrocephalus is a complex neurological disorder typically characterized by an abnormal accumulation of cerebrospinal fluid (CSF) within the ventricles of the brain and is the leading cause of neurosurgery in children across the globe (Figure 1; Munch et al., 2012; Kahle et al., 2016). While hydrocephalus can occur at any stage in life, pediatric cases with fetal and neonatal onset are particularly common, with an estimated incidence of approximately 1-2 babies out of every 1000 live births, and often result in the poorest neurological outcomes (Munch et al., 2012). Despite its many different causes, elevated intracranial pressure (ICP) in addition to ventricular dilatation is a common presentation across pediatric patients (Del Bigio, Wilson, & Enno, 2003). Numerous human and experimental animal studies of pediatric hydrocephalus have demonstrated severe and potentially irreversible impacts of ventricular dilatation on the white matter of the brain important for sustaining and developing various cognitive functions (Yuan et al., 2015; Yuan et al., 2016; Chumas et al., 1994; Del Bigio et al., 1994). Although the advent of modern surgical techniques used to divert CSF has drastically increased survival rates, pediatric hydrocephalus is still an incurable condition and many patients demonstrate residual cognitive deficits (Behjati, Emami-Naeini, Nejat, & el Khashab, 2011; Bigler, 1988; Hirsch, 1992; Mataro et al., 2001). Studies examining the outcomes of treated hydrocephalus have shown various cognitive impairments, with some appearing as early as infancy and persisting into adulthood, in domains such as verbal/non-verbal memory, language abilities, verbal/non-verbal intelligence and motor skills. However, deficits in higher-order executive functions appearing later in childhood and their relationship with early life white matter damage is still poorly understood (Fletcher et al., 1992; Fletcher et al., 1996; Hannay, 2000; Greene, 2014).

1.1 Pathophysiology

Although the pathophysiology of hydrocephalus is inherently complex due to its heterogenous etiology, the role of disrupted CSF dynamics is prominent across pediatric patients. CSF is a clear blood-plasma derived fluid predominantly secreted by the specialized

choroid plexus lining of the ventricles. In healthy individuals, CSF is continually secreted and flows throughout the ventricular cavities in a rostrocaudal direction via a series of narrow channels called foramina, until reaching its largest reservoir in the sub-arachnoid space (SAS). Once in the SAS, CSF flows in a multi-directional manner and is reabsorbed into the cerebral venous system through arachnoid granulations, where it can then re-enter systemic circulation (Dandy, 1919; Sakka, Coll & Chazal, 2011). Notably, up to a third of CSF is reabsorbed through cranial and spinal nerve sheaths, ultimately entering the lymphatic rather than the venous system (Sakka, Coll & Chazal, 2011). These alternative absorption pathways are believed to be especially active when the capacities of the cranial arachnoid villi are exceeded, or under the age of 18 months when the arachnoid villi have yet to become fully functional. Nevertheless, CSF circulation plays several important roles, such as regulation of normal brain development and function, regulation of brain interstitial fluid homeostasis and ICP, circulation of active molecules, and elimination of catabolites— all while providing hydromechanical protection and buoyancy for brain parenchyma (Lehtinen et al., 2011; Sakka, Coll & Chazal, 2011; Lehtinen et al., 2013).

The role of CSF obstruction in the development of hydrocephalus was recognized after the seminal experimental studies of Dandy and Blackfan (1914), who induced the dilatation of a dog's cerebral ventricles by placing a tiny obstructing body in the aqueduct of Sylvius, a canal which connects the third and fourth ventricles. Since their experiments, bulk-flow models where obstruction at any point along the CSF pathway can elicit an imbalance between secretion and reabsorption have become the standard approach to understanding hydrocephalus. Even nearly a century after Dandy and Blackfan's studies, the International Hydrocephalus Working Group describes hydrocephalus as the “active distension of the ventricular system of the brain resulting from inadequate passage of cerebrospinal fluid from its point of production within the cerebral ventricles to its point of absorption into the systemic circulation” (Rekate, 2008).

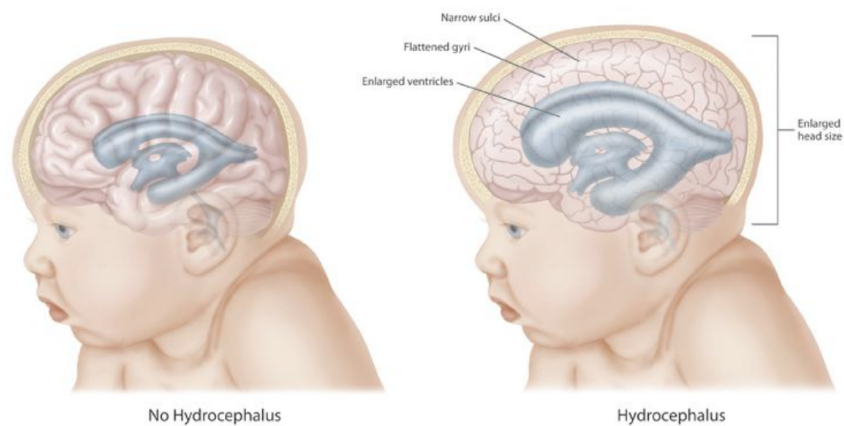


Figure 1. A schematic representation of CSF accumulation in the ventricular system of the brain in children with hydrocephalus. Typically, CSF which is continually produced in the ventricles flows back into systemic circulation and play several important roles for a healthy nervous system. When CSF flow is obstructed, intracranial pressure increases and the ventricular system can undergo rapid dilatation, severely impacting cortical and subcortical brain regions as well as periventricular white matter (From: Hydrocephalus, 2020).

In infants, disrupted CSF dynamics leading to hydrocephalus can result from a multitude of pathologies, ranging from congenital malformations arising in utero (e.g., Spina Bifida, Dandy-Walker Syndrome, aqueductal stenosis, neural tube defects, genetic abnormalities) or acquired brain lesions (e.g., intraventricular hemorrhage (IVH), infection, tumour, head trauma) which either obstruct adequate CSF flow within the ventricles or impair reabsorption into systemic circulation outside of the ventricles. When the cause of hydrocephalus is due to an obstruction of CSF flow within the ventricles it is known as obstructive or non-communicating hydrocephalus, whereas when an obstruction is not directly present within the ventricular system it is known as communicating hydrocephalus. For example, inflammation and scarring of the SAS due to infection or elevated pressure within the venous sinuses can impair reabsorption and lead to ventriculomegaly without actually obstructing

CSF inside the ventricles. Another form of hydrocephalus, although the rarest, can result from an excessive rate of secretion of CSF from the choroid plexus.

Recently, newer hydrodynamic models incorporating abnormal intracranial pulsations have also been proposed to account for hydrocephalus pathogenesis (Egnoe, Zheng, Rosiello, Gutman & Davis, 2002). CSF flow is pulsatile, following the systolic pulse wave in choroidal arteries, moving through the foramen magnum into the spinal SAS and then back into the skull with each heartbeat. Pulsatile CSF flow and return to systemic circulation can also occur along paravascular routes in brain parenchyma (Iloff et al., 2012), and mechanical amplification of pulsatile ventricular pressure waves synchronized with the cardiac cycle has been shown to illicit hydrocephalus in animal models (Pettorossi, Di Rocco, Mancinelli, Caldarelli & Velardi, 1978). In humans with hydrocephalus, altered pulsatility of CSF flow has been identified, but whether it is a cause or consequence of the disorder still remains in question (Wagshul, Eide & Madsen, 2011).

1.2 Clinical Presentation & Symptoms

In untreated hydrocephalus, continuous CSF secretion, reduced absorption and resistance to flow typically establishes an elevated ICP and ventriculomegaly that drives extensive structural displacement and distortion of the surrounding brain (Del Bigio, Wilson, & Enno, 2003). Although dependent on the mode of measurement, physiological values of intracranial pressure typically range between 3-4mmHg in infants, and higher values could reflect hypertension (Sakka, Coll & Chazal, 2011). In infants, high intracranial pressure will push the anterior fontanelle outwards as a tense bulge and can initiate an increasing head circumference while the sutures of the skull remain open. Macrocephaly, or a head circumference more than two standard deviations above the average for a particular age, presenting with splayed sutures and distension of the scalp veins is by far one of the most identifiable clinical signs of pediatric hydrocephalus. As a result of high pressure, some infants also show “sunsetting” of the eyes or an inability to produce an upward gaze. Other common symptoms include vomiting, behavioural changes, irritability, drowsiness, headaches, and loss of developmental milestones all with variable severity and progression across children and age of onset (Kahle, Kulkarni, Limbrick & Warf, 2016).

Monitoring changes in head circumference, intracranial pressure, ventricular volume and clinical presentation is crucial for the individualized management and intervention of hydrocephalus in children. For congenital cases, antenatal ultrasound (US) and magnetic resonance imaging (MRI) can detect malformations in the fetal brain, have normative data for ventricular size and allow serial investigation during gestation (Drake, 2008). For neonates and infants with open fontanelles, cranial US can be used to measure ventricular volume and detect lesions contributing to the individual case. Alternative neuroimaging techniques, such as MRI and computerized tomographic (CT) scans are also commonly used to assess the progression of the disorder where appropriate.

1.3 Shunt Treatment

For the past 60 years the most common treatment of hydrocephalus has been the surgical insertion of a permanent shunt which redirects CSF from the ventricles to another part of the body where it can become reabsorbed. Shunts have significantly reduced the mortality rate among patients and have also been shown to significantly improve physical and cognitive function (Chern et al., 2012; Gleichgerrecht et al., 2009). The development of shunts with magnetic adjustable pressure settings even after surgical placement has recently allowed neurosurgeons to fine tune intervention in a non-invasive manner. Most CSF shunts are comprised of three distinct parts, including: (1) a ventricular catheter inserted into the lateral ventricles; (2) a fixed pressure or adjustable valve to control the flow of CSF; and (3) a distal catheter which leads CSF to an external cavity. One of the most commonly used is the ventriculoperitoneal (VP) shunt, which allows CSF to travel out of the ventricles and down towards the abdominal cavity, however other CSF destinations such as the right atrium of the heart are also possible depending on the individual patient (Kahle, Kulkarni, Limbrick & Warf, 2016). Despite advances in shunt design, failure usually due to mechanical obstruction is a common occurrence, with about 40% of children needing some form of intervention within the first two years of original placement (Kulkarni et al., 2013). Another possible complication is shunt infection at about 5-9% per procedure and mostly occurs within 3 months of surgery (Kestle et al., 2011). Overall, a greater number of shunt revisions has been negatively correlated with cognitive outcome and quality of life (Hetherington, Dennis, Barnes, Drake & Gentili, 2005). While other treatment options exist, such as endoscopic

third ventriculostomy (ETV), the most typical goal of surgery is the diversion of CSF. The current study therefore focuses on outcomes related to children with VP shunts, however it is important to understand that etiology and individual patient history plays a role in terms surgical treatment options.

1.4 Impacts on White Matter

Numerous experimental animal models of hydrocephalus and human neuroimaging studies have demonstrated severe and multifactorial impacts of ventriculomegaly on white matter. As the ventricular system expands, extensive structural compression, displacement and distortion of the surrounding tissue can lead to secondary neurovascular damage, altered extracellular fluid homeostasis, and neuro-inflammation. Diminished cerebral blood flow predominantly in periventricular white matter is believed to contribute to the cascade of tissue injury and results in ischemic and hypoxic conditions that can further compromise brain development (McAllister, 2012; Harris & McAllister, 2011; Del Bigio, 2010). In Hydrocephalus-Texas (H-Tx) and Kaolin-induced rat models of hydrocephalus, decreased blood flow is associated with oxidative stress, lipid peroxidation, protein nitrosylation, and activation of calcium-dependent proteolytic enzymes that destroy axons (Socci et al., 1999; Del Bigio, 2000). In humans with hydrocephalus, studies of CSF content support evidence of hypoxic metabolism and lipid peroxidation, mirroring injury mechanisms similar to those seen in stroke and brain injury (Del Bigio, 1989; Krueger, 2004). Even in the acute stages of ventriculomegaly, oligodendrocytes responsible for producing myelin sheath undergo significant apoptosis in the surrounding white matter, and progressive ventricular dilatation only exacerbates the issue by eliciting reactive gliosis, including activation and proliferation of astrocytes and microglia, slowed axoplasmic transport, demyelination, axonal degeneration, and can result in a missing or malformed corpus callosum (Harris & McAllister, 2011; McAllister, Maugans, Shah & Truex, 1985; Welch & Lorenzo, 1991; Kahle et al., 2015; Khan, Enno & Del Bigio, 2006; Hanlo et al., 1997; Yuan et al., 2010; Welch & Lorenzo, 1991). Studies using diffusion tensor imaging (DTI) in humans and also experimental animal models have demonstrated the lasting negative impacts of hydrocephalus on myelination and cell proliferation, which may not be fully reversible after surgical CSF diversion (Chumas et al., 1994; Del Bigio et al., 1994; Del Bigio et al., 1997).

Overall the severity of white matter damage can be substantial and is thought to be mediated by factors such as the etiology, age of onset, ICP, rate of ventricular enlargement and size of the ventricles (Del Bigio, 2010).

1.5 Neurocognitive Outcomes Related to White Matter

Diffuse white matter damage characteristic of ventricular dilatation and high ICP has a multitude of impacts on neurocognitive outcome, however regional changes could also play more of a role than traditionally believed (Erickson, Baron & Fantie, 2010; Yuan et al., 2015; Yuan et al., 2016). In a study by Isaacs et al. (2009), DTI was used to investigate the microstructural differences in the lateral ventricular perimeter (LVP) and frontal-occipital horn perimeter (FOHP) in 13 infants with post-hemorrhagic hydrocephalus (PHH), 17 very pre-term infants with high-grade IVH without hydrocephalus, 56 full-term infants and 72 very pre-term infants without brain injury. Their findings highlighted prominent abnormalities in the PHH infants, including consistently lower fractional anisotropy (FA) and higher mean diffusivity (MD) than all other infants in the LVP and FOHP. Interestingly, within the PHH group, all DTI-related metrics indicated higher damage in the FOHP when compared to the entire LVP. The researchers interpreted this finding as the FOHP region being possibly subjected to higher stress in hydrocephalus because of its concave geometry and acute anterolateral angles, which could expand frontal and posterior extracellular spaces and facilitate tissue edema. Notably, studies using 3D ultrasound have shown that the posterior ventricular horns in pre-term hydrocephalus related to IVH dilate more than anterior horns, meaning there is potentially a stronger effect on the posterior white matter than the anterior portion (Kishimoto, Fenster, Lee, & de Ribaupierre, 2018; Qiu et al., 2016).

Another recent study by Yuan et al. (2016) using DTI tractography combined with graph theoretical analysis to examine topological structural connectivity changes in shunted pediatric hydrocephalus reported both global and regional network changes at 3- and 12-months post-surgery when compared to control children. Specifically, cortical regions such as the superior parietal gyrus, cingulate gyrus, medial frontal gyrus, medial occipital gyrus, and superior frontal gyrus, and subcortical regions such as the thalamus, caudate nucleus, and putamen, were all found to have significant abnormalities in regional network measures.

These regions are known to be involved in essential domains of motor and cognitive functions such as spatial processing, motor control, learning, memory, and executive functions (Dupont et al., 1994; Shulman et al., 1998; Briggs and Usrey, 2008; Tanaka et al., 2009; Renier et al., 2010; Schurz et al., 2013; Tu et al., 2013; Lester and Dassonville, 2014). One aspect that is possibly driving these frontal/posterior regional alterations could be the progressive pathophysiology of ventricular dilation in the FOHP.

In particular, the connectivity profile and white matter integrity of tracts connecting with the executive sub-region of the striatum requires further investigation. Corticostriatal circuitry projects to the striatum topographically, meaning the striatum has sub-regional specific functional and structural characterization with distinct areas shown to play a central role in coordinating different aspects of cognition, including motor and action planning, decision-making, motivation, reinforcement, and reward perception (Haber, 2016). While white matter damage has been a focus in many developmental and experimental studies, no existing human neuroimaging studies using DTI have explored the impact of surgically treated pediatric hydrocephalus on the integrity of regionally specific corticostriatal tracts in conjunction with the development of higher-order cognition later in childhood. As the FOHP has been shown to exhibit a higher degree of vulnerability to white matter damage, it could be possible that regional differences in frontal and posterior striatal tracts reflect this pattern of susceptibility.

1.6 Cognitive & Neuroanatomical Underpinnings of Executive Functions

Executive functions (EF) are a collection of distinct but interrelated higher-order, self-regulatory processes involved in planning, organizing, inhibiting and initiating behaviour as a means to solve complex problems, while monitoring and flexibly shifting problem-solving strategies when necessary (Alvarez & Emory, 2006). Individual differences in executive functioning skills measured in childhood are more predictive of physical and psychological health, substance dependence, financial well-being, social adjustment and criminal behaviour measured in adulthood than measures such as standardized IQ scores (Moffitt et al., 2011; Heckman 2006). In a clinical setting, EF is typically evaluated through ecologically validated

and standardized ratings which are easy to administer and interpret based on age and gender standardized norms, such as the Behaviour Rating Inventory of Executive Function (BRIEF2; Gioia, Isquith, Guy & Kenworthy, 2000), however there are also increasing efforts to employ validated performance-based measures in this setting.

Executive processes develop and change across the life span, and among healthy children the efficiency of the EF system is thought to improve in parallel to maturational changes in neural structures, including the ongoing myelination of neuronal axons connecting with the prefrontal cortex (Casey, Giedd & Thomas, 2000; Klingberg, Vaidya, Gabrieli, Moseley & Hedehus, 1999; Toga, Thompson, & Sowell, 2006). Functional MRI (fMRI) studies have recently highlighted brain regions implicated in distributed top-down cognitive control networks, such as the anterior cingulate cortex, dorsolateral prefrontal cortex, inferior frontal junction, anterior insular cortex, dorsal pre-motor cortex and posterior parietal cortex (Cole & Schneider, 2007; Dosenbach et al., 2007). In one study by Marek et al. (2019), which investigated 2188 children from 9-10 years old, resting state functional connectivity between several higher-order networks was related to general cognitive function.

Furthermore, the dorsal striatum has also been shown to play a prominent role in decision-making and higher-order processes (Cools & D'Esposito, 2011; Robertson, Hiebert, Seergobin, Owen, & MacDonald, 2015), and aberrant frontal-striatal connectivity and myelination with patterns of executive dysfunction has been repeatedly implicated in children with attention deficit hyperactivity disorder (ADHD; Swanson, Castellanos, Murias, LaHoste & Kennedy, 1998). Interestingly, researchers have also recently reported a high degree of comorbidity of hydrocephalus and ADHD, where children with hydrocephalus are significantly more likely to be diagnosed with ADHD in comparison to healthy controls (Burmeister et al., 2005; Brewer et al., 2001). Indeed, impairments in performance-based assessments of executive functions have been reported in children with hydrocephalus, including deficits in goal-directed behaviour, focusing, processing speed, and shifting attention. However, no study to date has investigated the possibly related striatal white matter abnormalities using DTI or MT imaging (Brewer et al., 2001; Fletcher et al., 1996; Mahone et al., 2002).

1.7 Diffusion Tensor Imaging

While conventional MRI techniques, such as T1-weighted imaging and T2-weighted imaging, are able to detect major structural abnormalities, these protocols lack the sensitivity and specificity to address microstructural white matter abnormalities. Diffusion tensor imaging (DTI) is an advanced *in vivo* MRI technique that quantifies the microscopic diffusivity properties of water molecules in the brain. As water diffusion is inherently more restricted in white matter than in other compartments of the brain due to the hindering presence of axonal membranes, DTI can be used to map out fiber tracts and reconstruct structural connections by computer algorithms such as probabilistic tractography (Behrens et al., 2003; Behrens, Johansen-Berg, Jbabdi, Rushworth & Woolrich, 2007). DTI metrics such as fractional anisotropy (FA) and mean diffusivity (MD), which respectively measure the degree of asymmetry in diffusion and the average magnitude of diffusion in each voxel, are able to detect axonal degeneration on the microscopic scale, and have been shown to be correlated with immunohistochemical biomarkers of white matter cytopathology in a rat model of hydrocephalus (Yuan et al., 2010). Higher FA can reveal more hinderance in water diffusion to a specific axis, and is interpreted as higher white matter integrity, while the opposite is true for MD. Several studies using DTI to measure FA and MD in patients with hydrocephalus have revealed remarkable differences between patients and healthy children that persist even post-shunt treatment (Air et al., 2010; Assaf et al., 2006; Isaacs et al., 2019; Mangano et al., 2016; Scheel, Diekhoff, Sprung, & Hoffmann, 2012). However, FA and MD are still only non-specific markers for neurodegeneration, and adequate biological interpretation of these diffusion measures requires a more detailed analysis. Probing additional DTI metrics such as axial diffusivity (AD), the principal diffusivity eigenvalue, and radial diffusivity (RD), the average magnitude of diffusivity perpendicular to the principal diffusivity vector, allows for the disentanglement of demyelination from general axonal damage. Thus, a multivariate DTI approach supports a more nuanced understanding of the underlying microscopic white matter changes and can aid in the understanding of related neurocognitive outcome.

1.8 Magnetization Transfer Imaging

White matter demyelination patterns have also been quantified in various clinical populations using another *in vivo* MRI technique called magnetization transfer (MT) imaging, which is able indirectly detect levels of lipids and other macromolecules with the magnetization transfer ratio (MTR; Crespy et al., 2011; Hähnel et al., 1999). MTR is a measure of magnetization exchange between macromolecule-bound and free protons and has been used to monitor changes in the developing brain and estimate myelination processes (Bagnato & Frank, 2003; Zaaraoui et al., 2008). One study using Kaolin-induced hydrocephalus in rats showed that pre- and post-shunting MTR values were associated with neurological and behavioural changes (Catalão et al., 2014). However, the only human neuroimaging studies to have investigated white matter changes in hydrocephalus using MTR have been conducted on adult-onset patients, or individuals with an already totally myelinated brain (Hähnel et al., 1999; Hähnel et al., 2000). Therefore, this thesis will be the first study to investigate MTR in growing sample of children with pediatric-onset hydrocephalus, in addition to DTI.

1.9 Current Study

While previous studies have identified patterns executive dysfunction in children with hydrocephalus, the role of striatal white matter damage in relationship to these findings using DTI has yet to be investigated. Given the particular vulnerability of the developing brain to ventriculomegaly and the potentially irreversible white matter impacts post-surgical intervention, it is possible that deficits in higher-order cognitive functions are related to altered structural connectivity and integrity within cortico-striatal networks. The current pilot study's objective was thus to investigate the long-term white matter correlates of shunted hydrocephalus in cortical-striatal circuitry and to investigate executive functioning outcomes measured through parental reports on the Behaviour Rating Inventory of Executive Functioning (BRIEF2; Gioia, Isquith, Guy & Kenworthy, 2000). The study was conducted with a small sample of children with hydrocephalus who were treated within their first year of life with a fixed valve VP shunt, and with larger sample of age-matched neurotypically developing controls. White matter integrity and structural connectivity between the executive sub-region of the striatum and the cortex was assessed by means of DTI, a non-invasive *in*

vivo neuroimaging technique which allows for reconstruction of structural networks via probabilistic tractography. Additionally, the magnetization transfer ratio for a smaller number of children was assessed to complement the DTI-related findings of white matter integrity. The relationship between white matter findings and executive functioning outcome was also investigated.

OBJECTIVE: To investigate the executive functioning outcomes and changes in white matter connectivity and integrity in school aged children with VP shunted hydrocephalus and age-matched healthy developing controls.

HYPOTHESIS: White matter damage in cortico-striatal circuitry due to ventricular dilatation in pediatric hydrocephalus is associated with impaired development of executive functions in childhood.

RESEARCH AIMS:

1. To assess executive function outcomes at school age in children with VP shunted hydrocephalus and healthy controls.
2. To investigate cortico-striatal differences in structural connectivity and white matter integrity (FA, MD, AD, RD, and MTR) between children with hydrocephalus and healthy controls.
3. To investigate the relationship between white matter integrity and executive function outcome in children with shunted hydrocephalus.

Studies investigating long term outcomes in clinical pediatric samples frequently pose analytical challenges related to small sample size and non-normal distributions (Button et al., 2013; Wright, London & Field, 2011). Standard approaches to hypothesis testing such as parametric univariate statistical tests often rely on the assumption of normally distributed and are not always appropriate for small clinical samples. The bootstrap test, originally developed by Tibshiani and Efron (1993), is a data-based resampling statistical method that can be used to construct a sampling distribution of a test statistic. Given this distribution, the precision of the statistic can be estimated and the probability of obtaining a single value can be calculated

(Wilkinson et al., 1999; Wright, 2003). The current study will thus implement the bootstrap technique to test how individual patients correlate with a normative profile of structural connectivity and integrity generated using the larger sample of age-matched controls.

Chapter 2

2 Methods

2.1 Participants

All participants were invited to take part in a two-session, behavioural MRI study over a total of 3 hours at Western University. Healthy controls were recruited through the Developmental Research Participant Pool and the OurBrainsCAN Cognitive Neuroscience Research Registry. Both databases are of London, Ontario families who voluntarily participate in psychological research at Western University. Parental written consent was obtained for their child's participation and children provided verbal assent. Parents were reimbursed for travel and parking related expenses. All protocols were approved by Western's Research Ethics Boards (REB; Appendix A).

2.2 Patients with Hydrocephalus

Ten patients were recruited from a follow-up paediatric neurosurgery clinic in the London Health Science Centre run by Dr. de Ribaupierre. All patients were clinically stable at time of recruitment and were treated with a VP shunt within the first year of life. Out of the ten patients, six successfully completed our neuroimaging protocol and ranged from 6-10 years of age ($M= 8.43$ years, $SD= 1.61$). All patients who completed the DTI protocol are denoted with an asterisk in Table 1, where additional clinical details are also available. Patient 4A completed the entire protocol a second time, almost a year later (356 days) as Patient 4A2 and is included in the behavioural/imaging analysis.

<i>Patient</i>	<i>Age (years)</i>	<i>Sex</i>	<i>Prematurity (weeks)</i>	<i>Birth-weight</i>	<i>Etiology</i>	<i>Age of Onset</i>	<i>Treatment</i>	<i># Shunt Revisions</i>
<i>1A</i>	5.42	M	Yes (25)	XLBW	IVH	Birth	VP shunt	0
<i>2A*</i>	9.92	M	No	Normal	IVH	4 months	VP shunt	0
<i>3A</i>	5.33	M	Yes (27)	VLBW	IVH	Birth	VP shunt	0
<i>4A*</i>	6.25	M	No	Normal	DWM	3 weeks	VP shunt	0
<i>5A*</i>	8.92	M	Yes (26)	XLBW	IVH + MG	Birth	VP shunt	0
<i>6A</i>	11.33	M	Yes (28)	VLBW	IVH	Birth	VP shunt	3
<i>7A*</i>	10.08	F	No	Normal	SB	1 week	VP shunt	0
<i>8A*</i>	6.83	M	No	Normal	N/A	8 months	VP shunt	0
<i>9A*</i>	9.75	M	No	Normal	SB	1 week	VP shunt	2
<i>10A</i>	5.75	F	Yes (26)	LBW	IVH	Birth	VP shunt	3

Table 1. A list of all patients recruited for the study, with patients who were able to complete the diffusion neuroimaging protocol denoted with an asterisk (*). LBW= low birth weight, VLBW= very low birth weight, XLBW=extra low birth weight, IVH = Intraventricular Hemorrhage, DWM= Dandy-Walker's Malformation, MG= meningitis, SB= Spina Bifida, and VP= ventriculoperitoneal.

2.3 Control Group

Twenty-two neurotypically developing children (12 females) were recruited as healthy controls. Ages ranged from 6-10 years old, and the mean age was not significantly different from that of the patient group ($M= 8.35$ years old, $SD=1.54$, $p= .455$). Three controls were unable to complete the diffusion MRI protocol and were thus excluded from the neuroimaging analysis.

2.4 Socioeconomic Status

Parental socioeconomic status (SES) is a particularly important variable to control for when studying neurodevelopment, especially in clinical pediatric samples, as low SES has repeatedly been associated with adverse neurocognitive outcomes in children with brain injury (Benavente-Fernández et al., 2019). Factors that contribute to SES include maternal education, single parent families, parental occupation, familial support and social environment. Measures of parental SES were obtained for every participant using the Hollingshead Four Factor scale, which assesses maternal and paternal educational and occupational status (Cirino et al., 2002). On this scale, scores of parental SES range from 8 to 66, with low SES represented anywhere from 8 to 20 and average SES represented anywhere above 21. A t -test of parental SES scores revealed no group differences between our patients and controls ($M_{patients}= 45.71$, $SD_{patients}= 11.67$, $M_{controls}= 47.52$, $SD_{controls}= 13.15$, $p=.367$).

2.5 Behaviour Rating Inventory of Executive Functions

Parental reports of everyday functioning within the past 6 months were obtained using the Behavioural Rating Inventory of Executive Functions (BRIEF2; Gioia, Isquith, Guy & Kenworthy, 2000). The BRIEF is an ecologically valid assessment of behaviour outside the laboratory setting and a golden standard used in a wide range of childhood disorders (Mahone et al., 2002; Mahone, Zabel, Levey, Verda & Kinsman, 2010). Responses are scored into sub-domains of executive functioning, which are combined into a Behaviour Regulation Index (BRI), Emotional Regulation Index (ERI), Cognitive Regulation Index (CRI), and an overall Global Executive Composite (GEC; Figure 2). All raw scores are

converted into age and gender standardized *t*-scores, with higher scores indicating greater executive dysfunction. *T*-scores were interpreted according to Table 2.

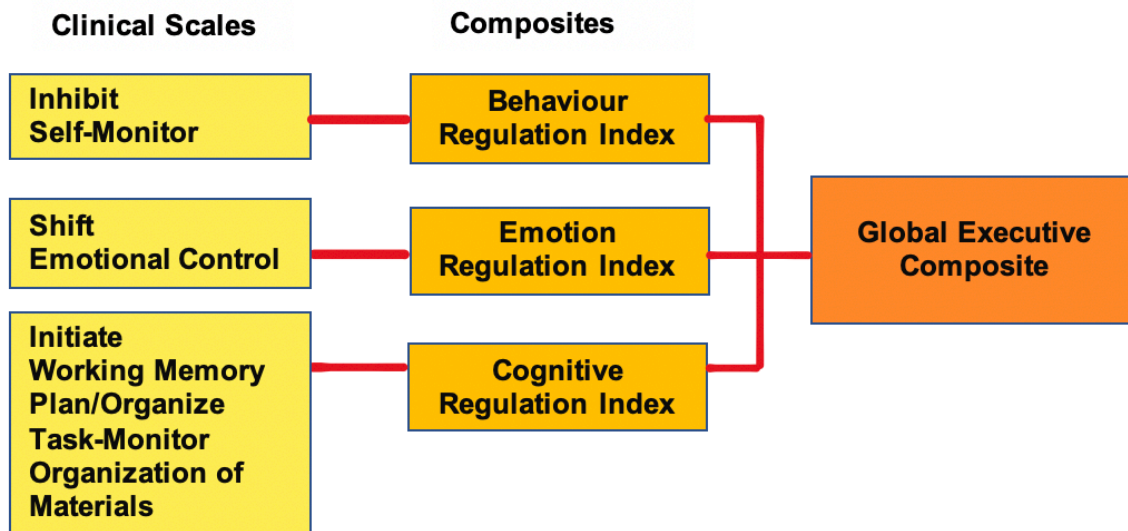


Figure 2. Schematic representation of the clinical scales and respective composite scores measured by parental reports on the Behaviour Rating Inventory of Executive Function (BRIEF2). For the current study, the three composite scores (Behaviour Regulation Index, Emotion Regulation Index, and Cognitive Regulation Index) as well as the Global Executive Composite score was investigated in patients and controls.

<i>T-score</i>	<i>Standard Deviation</i>	<i>Interpretation</i>
$T = 50$	0	Mean Score
$60 < T < 64$	1-1.5	Mildly Elevated
$65 < T < 69$	1.5-2	Potentially Clinically Elevated
$70 < T$	2	Clinically Elevated

Table 2. Interpretation of age and gender-standardized *t*-scores was based on the following guidelines obtained from the BRIEF2 scoring manual. A *t*-score of 50 represented the mean score of the normative population, with increasing scores representing higher degrees of executive dysfunction.

2.6 Neuroimaging Protocol

In order to mitigate possible fear and discomfort, both patients and controls were first exposed to a 10-15 min mock scan that simulated the space and sound of the real MRI machine. During this training session, all participants were instructed to stay as still as possible and younger children were encouraged with a visual storybook describing the process. All participants were instructed in the use of a button to signal discomfort/fear while in the real scanner. Between image series in the real MRI, verbal feedback was provided over an intercom system to help mitigate motion in our pediatric sample (Greene et al., 2018). During image acquisition, participants watched short films with audio-visual signal, which has also been shown to decrease motion artifact (Vanderwal, Kelly, Eilbott, Mayes, & Castellanos, 2015).

MRI images were acquired in a second session at the Robarts Research Institute at the University of Western Ontario using a 3-Tesla Siemens Magnetom Prisma Fit scanner and a Siemens Prisma 32-channel head coil. The entire imaging protocol lasted approximately 1 hr

15 min, and included diffusion imaging, high-resolution T1-weighted imaging, magnetization transfer imaging as well as task-based and resting state functional MRI which has been reported previously by Hashi (2019).

2.7 Structural & Diffusion MRI Acquisition & Parameters

The imaging protocol began with a localizer scout image used to orient the subject and proceeded with two consecutive series of diffusion weighted echo-planar imaging (DWI) obtained in opposite phase-encoding directions along the anterior-posterior axis. Diffusion volumes were obtained with the following parameters: gradient directions= 30; b-value= 1000s/mm²; isometric voxel size= 2×2×2 mm³; and matrix size= 192×192 mm. For each DWI series, a single volume referred to as the b0 was acquired without diffusion weighting (b-value= 0 s/mm²).

Next, a high-resolution T1-weighted anatomical image was acquired using a three-dimensional magnetization-prepared rapid acquisition with gradient echo (MP-RAGE) sagittal pulse sequence, with the following parameters: repetition time (TR)= 2300ms; echo time (TE)= 2.93 ms; flip angle= 9°; matrix size= 256×256 pixels; and where one whole brain image consisted of 160, 1 mm-thick slices. The field of view of the anatomical image was oriented along the anterior and posterior commissure with a matrix of 256×256 pixels and a 1×1×1mm³ isotropic voxel size. Once the T1-weighted image was collected, the exact same DWI series reported above was replicated, resulting in a total of four DWI series

At the end of the imaging protocol, a portion of children were able to complete magnetization transfer (MT) imaging, including 11 controls and 3 patients. The MT images were acquired using 3D gradient recalled echo sequence (GRE) with the following parameters: TR= 28 ms; TE= 2.87ms; flip angle= 10°; FOV= 256 mm; matrix= 256 × 256; 1×1×1mm³ isotropic voxel size; bandwidth= 260 Hz/Px; and where one whole brain image consisted of 144, 1 mm-thick slices. MTR was calculated by acquiring the sequence twice – once with an off-resonance MT transfer pulse (MT_{OFF}) and once without (MT_{ON}).

2.8 Image Preprocessing

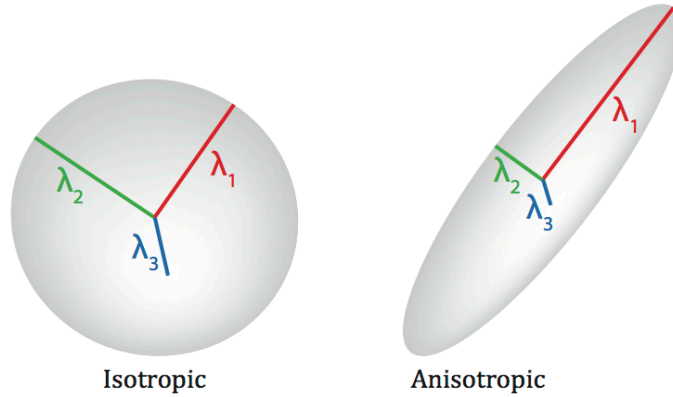
All preprocessing steps were implemented using the standard FMRIB Software Library (FSL) v6.0.3 FDT toolbox (Smith et al., 2001), compiled and customized within a shell script to parallelize processing across participants. Structural, MTR, and diffusion images were first converted from Digital Imaging and Communications in Medicine (DICOM) format to Neuroimaging Informatics Technology Initiative (NIfTI) volumes and organized into Brain Imaging Data Structure (BIDS) using dcm2bids (<https://github.com/cbedetti/Dcm2Bids>; Gorgolewski et al., 2016). T1-weighted anatomical images were then skull-stripped iteratively using robust brain centre estimation with BET, and a binary brain mask was generated. Volumes with skull-brain interface outlines were visualized using FSLeaves to ensure correct brain extraction, and failures were corrected at the individual subject level. Next, b0 volumes were extracted from every diffusion series and concatenated into a single volume that was used for susceptibility-induced distortion correction with TOPUP. All 4 DWI series were concatenated into a single image, along with the respective metadata in the bvals and bvec files. This approach was taken to increase the signal to noise ratio (SNR) for tensor estimation. Subject movement was corrected by linear registration to the first b0 volume and eddy current induced distortion correction was applied using FSL's eddy.

2.9 Tensor Estimation

Diffusion tensor models were fit at each voxel within the pre-processed diffusion volumes to obtain maps of corresponding eigenvectors (ϵ_1 , ϵ_2 , and ϵ_3) and eigenvalues (λ_1 , λ_2 , and λ_3) using DTIFIT. Measures of fractional anisotropy (FA), an index for the amount of diffusion asymmetry, and mean diffusivity (MD), the average diffusivity across all three eigenvalues, were also obtained at the voxel level, along with axial diffusivity (AD) and radial diffusivity (RD; Figure 3).

An overlay of the primary diffusivity vector onto an FA volume was visualized using FSLeaves to ensure successful estimation of the tensor for each subject (Figure 4). To prepare data for probabilistic tractography, preprocessed data underwent Bayesian Estimation of

Diffusion Parameters Obtained using Sampling Techniques (BEDPOSTX), with modelling of crossing fibers at the voxel-level.



$$\text{Fractional Anisotropy (FA)} = \sqrt{\frac{(\lambda_1 - \lambda_2)^2 + (\lambda_2 - \lambda_3)^2 + (\lambda_1 - \lambda_3)^2}{2(\lambda_1^2 + \lambda_2^2 + \lambda_3^2)}}$$

$$\text{Mean Diffusivity (MD)} = (\lambda_1 + \lambda_2 + \lambda_3)/3$$

$$\text{Axial Diffusivity (AD)} = \lambda_1$$

$$\text{Radial Diffusivity (RD)} = (\lambda_2 + \lambda_3)/2$$

Figure 3. Schematic of the diffusion tensor model calculated within each voxel of diffusion weighted volumes. Fractional anisotropy is a scalar value calculated as the square root of the sum of squares (SRSS) of the diffusivity differences, divided by the SRSS of the diffusivities. FA values closer to 1 represent higher white matter integrity. Mean diffusivity is calculated as the average of all three eigenvalues in mm²/s. Axial diffusivity represents the principal diffusion vector, and is equal to the first eigenvalue in mm²/s. Radial diffusivity represents diffusion perpendicular to the largest eigenvalue, and is calculated as the average of the second and third diffusivity eigenvalue in mm²/s.

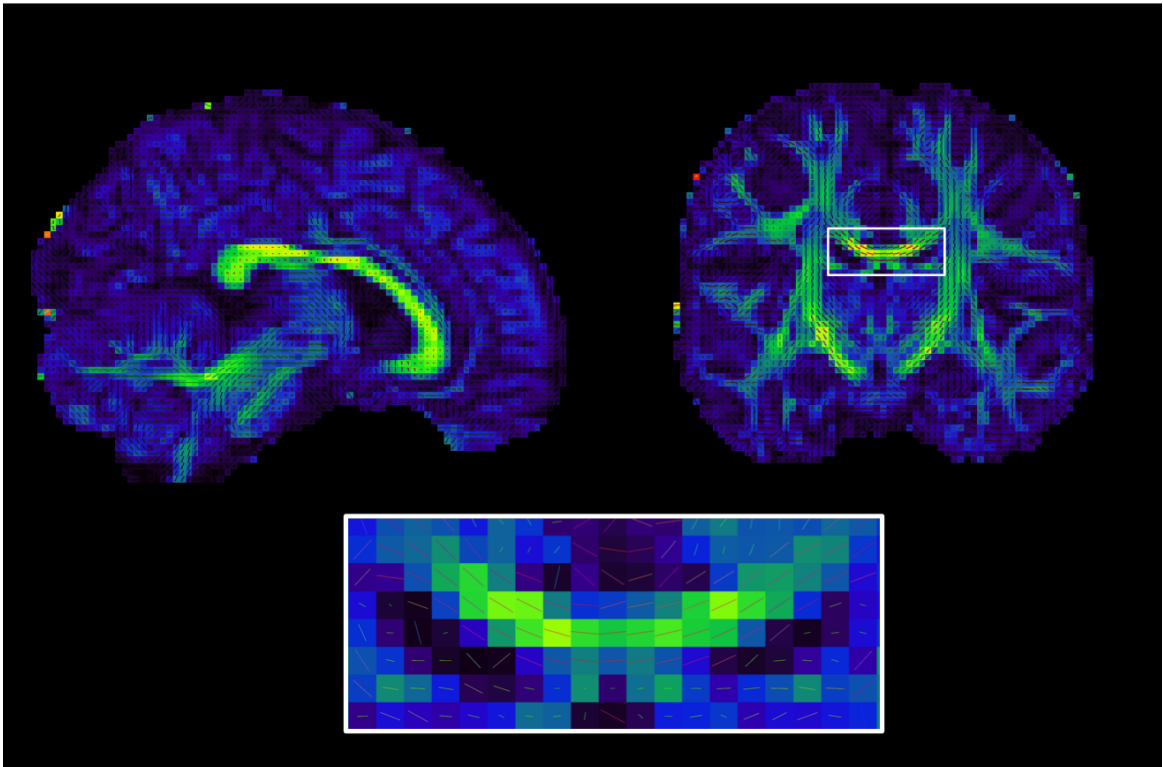


Figure 4. Principal diffusivity vector maps modulated by fractional anisotropy were viewed for each subject during pre-processing to ensure correct tensor estimation before tractography. Higher FA is shown in yellow-green and the principal diffusivity vector (ϵ_1) is shown within each voxel. Correct tensor estimation was determined by examining the corpus callosum (as seen in the bottom-most panel) on a coronal slice.

2.10 MTR estimation

Magnetization transfer ratio (MTR) imaging measures the presence of macromolecules in tissue, including the high lipid content found in myelin, and can be used to indirectly extract information on white matter integrity and myelination in addition to DTI. This is achieved by acquiring two sets of images: 1) an image with an off-resonance radiofrequency (RF) pulse designed to saturate protons bound to macromolecules but not those in free-water; and 2) another image with a RF pulse at the Larmor frequency of the free-water protons. Due to the

partial transfer of magnetization from the macromolecule-bound to free-water protons via dipole-dipole interactions, the signal from free water protons is reduced secondary to this effect. The difference between the signals acquired with and without the off-resonance pulse can be computed as the MTR as follows:

$$\text{MTR} = (\text{MT}_{\text{OFF}} - \text{MT}_{\text{ON}}) / \text{MT}_{\text{OFF}}$$

Where higher MTR values are associated with higher myelination and lower MTR values are indicative of demyelination.

2.11 Harvard-Oxford Cortical FSL Atlas

Forty-eight cortical regions were parcellated in subject-level diffusion space through a series of linear and non-linear transformations with nearest-neighbours interpolation (FLIRT/FNIRT). First, the Harvard-Oxford Cortical FSL Atlas was transformed from the original adult MNI152-2mm space to two age-specific paediatric templates, ranging from: 4.5-8.5 and 7.5-13.5 years old (Fonov, Evans, Botteron, Almli, McKinstry, Collins & BDCG, 2011; Fonov, Evans, McKinstry, Almli & Collins, 2009). Registration from diffusion space to this age-specific standard space was a two-step process, using the subject's structural T1 image as the mid-point reference and concatenating the two steps to minimize resampling. Non-linear transformations were performed with a multi-resolution approach consisting of 8 subsampling schemes (16,8,4,4,2,2,1,1 subsamples), moving towards higher resolution and lower levels of smoothing with a full-width at half maximum (FWHM) Gaussian filter (8,8,6,5,4,2,0,0 mm) within each scheme. The resulting warp was then inversed and applied to the atlas in the age-specific standard space in order to parcellate cortical regions in native diffusion space (Figure 5). Visual inspection of volumes along the registration pathway in FSLeyes confirmed successful parcellation in all subjects, and registration failures were troubleshooted with alternative parameters.

2.12 Oxford-GSK-Imanova Striatal Connectivity FSL Atlas

The same procedures used to segment cortical regions outlined above were implemented on the Oxford-GSK-Imanova Striatal Connectivity FSL Atlas to achieve striatal parcellation in diffusion space (Figure 5). Seven distinct striatal subregions (including caudal-motor, limbic, rostral-motor, executive, parietal, occipital, and temporal regions) were defined on the basis of structural connectivity with cortical regions in Tziortzi et al. (2013). For example, the executive sub-region was defined by high connectivity probability with Petrides' (2005) functional areas 9, 9/46 and area 10 of the dorsolateral prefrontal cortex, while the caudal-motor sub-region was defined by high connectivity probability with the primary motor cortex (area 4) and the caudal premotor area (caudal area 6).

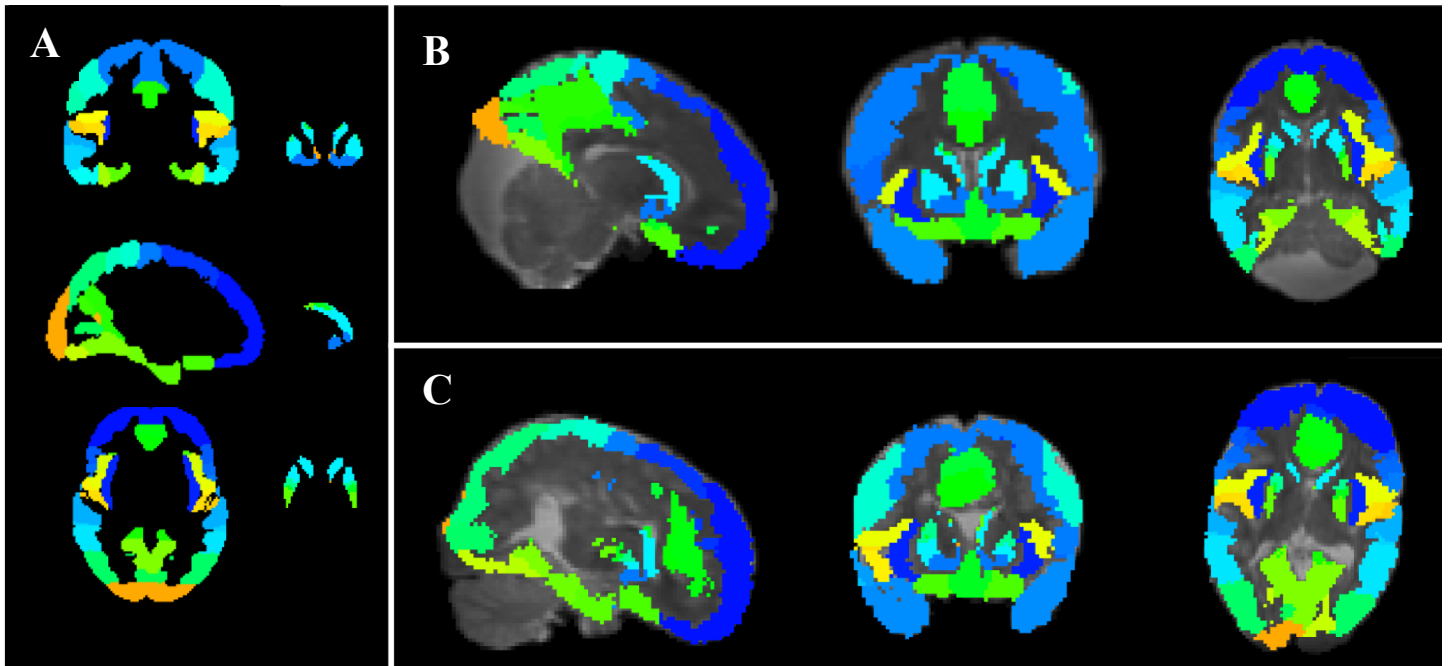


Figure 5. Mask image of the 48 regions of interest (ROIs) from the Harvard Oxford Cortical Atlas and the 7 sub-cortical ROIs obtained from the Oxford-GSK-Imanova Striatal Connectivity FSL Atlas before non-linear transformation into native diffusion space for patient 4A (B) and patient 5A (C).

2.13 Probabilistic Tractography

Probabilistic tractography was performed *in vivo* to investigate structural connectivity between 7 striatal and 48 cortical regions and obtain volumetric maps of cortical-striatal

tracts (probtrackx2). The tractography algorithm was applied with default parameters (step length= 0.5, steps= 2000, curvature threshold= 0.2) to iteratively sample 5000 streamlines per seed mask voxel, each time stepping in the most likely direction by sampling diffusivity tensors in local voxels. In this stepwise manner, a probabilistic streamline to the target is generated, where voxel values represent tract density and the proportion of successful streamlines is indicative of structural connectivity between regions (Behrens et al., 2003; Behrens, Johansen-Berg, Jbabdi, Rushworth & Woolrich, 2007). All cortical and striatal ROIs were used as exhaustive seed/target pairs to construct a 55×55 matrix containing the number of successful streamline counts. As the diffusion tensor is a voxel-averaged quantity, dMRI is not able to determine anterograde/retrograde connectivity at the cellular level regardless of image resolution (Bammer, Acar, Moseley, 2003)— thus a bi-directional index of structural connectivity was obtained by taking the average number of streamlines between seed/target pairs to construct a symmetrical matrix along the diagonal.

Probabilistic streamline counts have been shown to be sensitive to variability in seed and target ROI sizes (Cheng et al., 2012). In our sample, ROI size variability existed both within and between subjects partly due differences in warping required for parcellation in native diffusion space. To correct for this intra and inter-subject variability in ROI size, the following was computed:

$$\text{Connectivity Index} = \frac{\text{Successful Streamline Count}}{(\text{Seed ROI voxels} + \text{Target ROI voxels})/2}$$

Where the connectivity index between any two ROIs is now equal to the successful streamline count divided by the average number of voxels in both ROIs. This bi-directional, corrected connectivity index was used as input to the threshold connectivity networks and for all structural connectivity statistical tests.

Saved striatal-cortical tract volumes were defined by voxels containing streamline densities above the 10th percentile, and gray-matter represented in seed regions was subtracted out. The tracts included in the 7 striatal-cortical networks described below were then used to isolate metrics of white matter integrity. This was done by binarizing tract volumes into a mask image that would be used extract FA, MD, AD, and RD in diffusion space and

transformed to magnetization transfer imaging space to extract MTR values. Extracted values of FA, MD, AD, RD and MTR were then averaged along all voxels within each striatal-cortical tract to obtain a single representative metric

2.14 Patient Shunts

After a preliminary first pass of probabilistic tractography, visual inspection revealed patient 5A had streamlines flowing through their shunt (Figure 6A), possibly influencing the connectivity values obtained for regions local to the shunt. To avoid the possibility of streamlines following the directional diffusion of water along shunts, tractography was re-run for all patients with manually segmented 3D shunt masks used to terminate streamlines. Shunt segmentation was performed on a single-voxel level using an overlay on T1-weighted images with FSLEyes with a 2-mm spherical dilation (Figure 6B). After transforming the binary mask into diffusion space, visual inspection of overlap with shunt streamlines from previous tractography results was confirmed. Successful mapping of the shunt was reviewed and confirmed by a pediatric neurosurgeon along coronal, axial and horizontal slices in T1-weighted space.

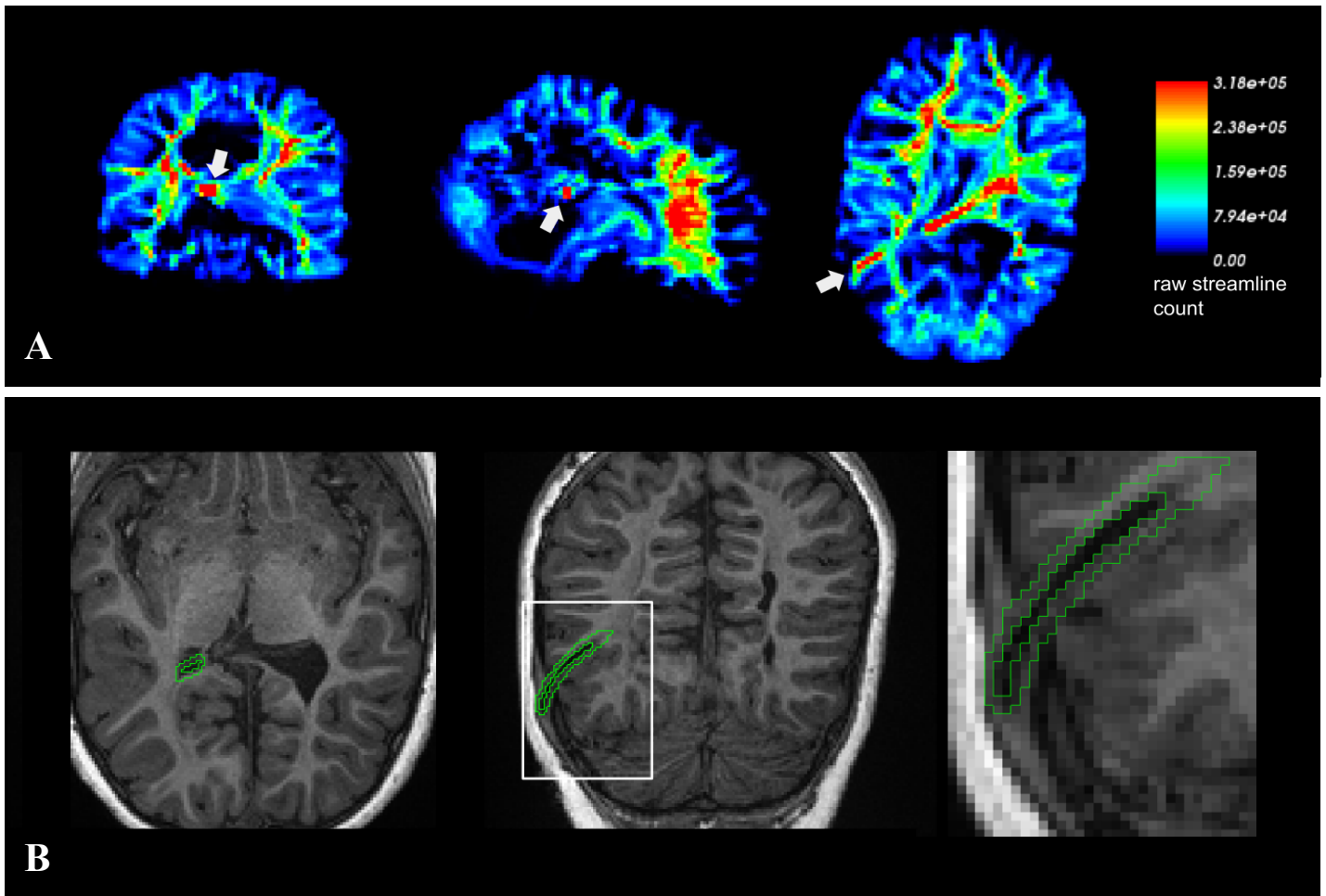


Figure 6. Output of whole-brain probabilistic tractography for patient 5A, where voxels are coloured according to their raw streamline density. Blue voxels represent low streamline density whereas red represent high streamline density. Preliminary visual inspection of tractography revealed streamlines generated in line with the patient’s CSF shunt, highlighted with the arrow in coronal, sagittal, and axial slices (A). Manual segmentation of the patient’s shunt using an overlay on the T1-weighted image was then used to create a binary mask (green outline), which was dilated by 2-mm before transforming into diffusion space. This mask was then used as input to stop tracking streamlines if they entered this location (B). Manual shunt segmentations were performed for every patient.

2.15 Isolating Sub-Striatal Networks

Spurious connections between two ROIs which are not “truly” anatomically connected may arise when using probabilistic tractography (de Reus and van den Heuvel, 2013; Girard et al., 2014). One approach to resolve false positives in connectomic studies has been to pool individual subjects into a group average connectivity matrix to obtain a stronger signal to noise ratio, and then apply some threshold based on a desired density to isolate the strongest estimates of connectivity (Hagmann et al., 2008, Perry et al., 2015; Rubinov & Sporns, 2010). Thus, to isolate the 7 distinct striatal-cortical structural networks in the current study, a streamline-informed approach was taken following the methodology of Tziortzi et al. (2013) and Crosson et al. (2005). In brief, a threshold was used to exclude tracts on the basis of their corrected bi-directional connectivity value in the group average profile. This was accomplished by rank-ordering connectivity to all 48 possible cortical regions from individual striatal-subregions and excluding tracts with connectivity below a certain value. Visual inspection confirmed a reasonable threshold level at 10% of the maximum connectivity value within each network (Appendix B). Using this approach, networks were not dependent on a pre-defined density value at the entire connectome level and were able to have some degree of overlapping targets.

2.16 Statistical Analysis

All statistical analyses were performed in MATLAB-R2019b. Patients with hydrocephalus were compared to the control group in terms of striatal-cortical network connectivity, dMRI-assessments of white matter, and MTR. Visual inspection of each patient profile within the isolated networks, and comparison to the control group mean profile with 95% confidence intervals constructed using *t*-scores, was used to identify trends in the data. Rather than implementing a series of under-powered conventional univariate tests to identify specific tracts that set apart the 7 patients from 19 controls, a multivariate approach was taken by correlating entire patient white matter profiles with the control group mean profile to identify dissimilarity in FA, MD, AD, RD, and MTR values across all included tracts. Furthermore, due to the heterogeneity of the patient population, a case-approach was taken to treat each patient as an individual and to identify the likelihood of each patient’s correlation by

comparison with a distribution of correlation co-efficients bootstrapped from an age-matched sample of healthy controls.

2.17 Bootstrapped Correlation Distribution

Correlations of every individual within the control group on metrics of connectivity, FA, MD, AD, RD, and MTR were bootstrapped to a random control mean profile, sampled with replacement 10,000 times from the entire control pool while excluding the individual control in question (Figure 7). The resulting distribution containing 190,000 correlation coefficients was used to identify the probability of obtaining a correlation co-efficient for each individual patient. Connectivity, FA, MD, AD, RD and MTR profiles within each patient's executive striatal-cortical network was correlated to the control group mean profile and plotted within the bootstrapped distribution of correlation coefficients obtained using the procedure outlined above.

For statistical analyses of white matter metrics, $p < 0.05$, corrected for multiple comparisons using Bonferroni correction, was used as the statistical threshold where applicable. The corrected p -value of 0.01 was used for tests investigating white matter integrity and was obtained by dividing the critical value by 5 (the number of white matter metrics under investigation: FA, MD, AD, RD, and MTR).

2.18 FA Linear Regression with GEC Scores

To minimize the number of tests and avoid being under-powered, only FA-correlations were chosen to assess the linear relationship of aberrant white matter integrity with GEC scores. Lower correlations represented higher dissimilarity with the control mean profile, and higher GEC scores derived from parental reports on the BRIEF2 represented higher executive dysfunction. A total of two regressions were thus performed on FA-correlations derived from: (1) the striatal-executive network; and (2) the striatal-occipital network. The regression with the striatal-occipital network was performed as a negative control to investigate the specificity of the findings to the striatal-executive network.

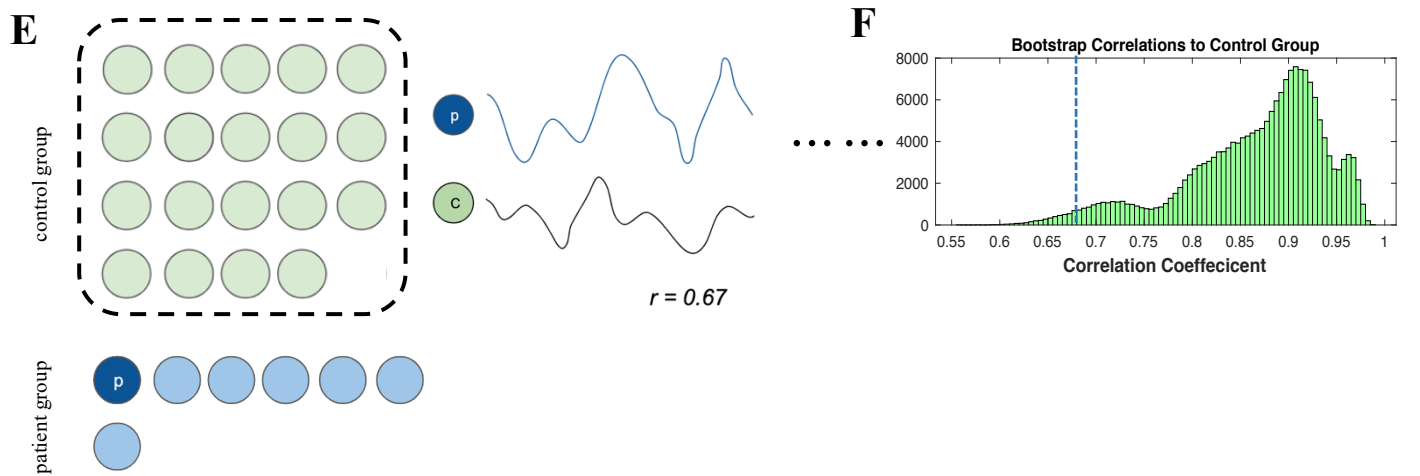
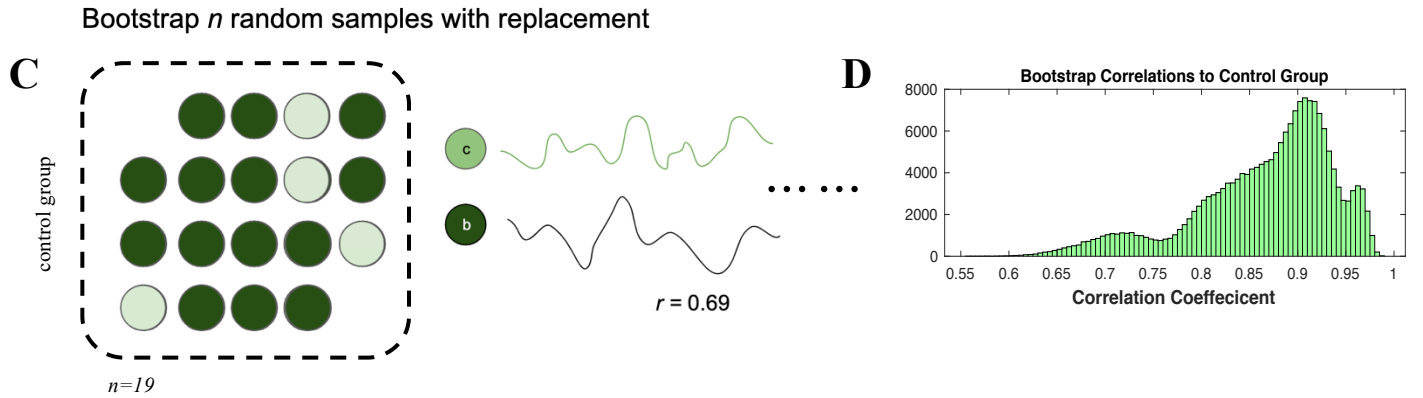
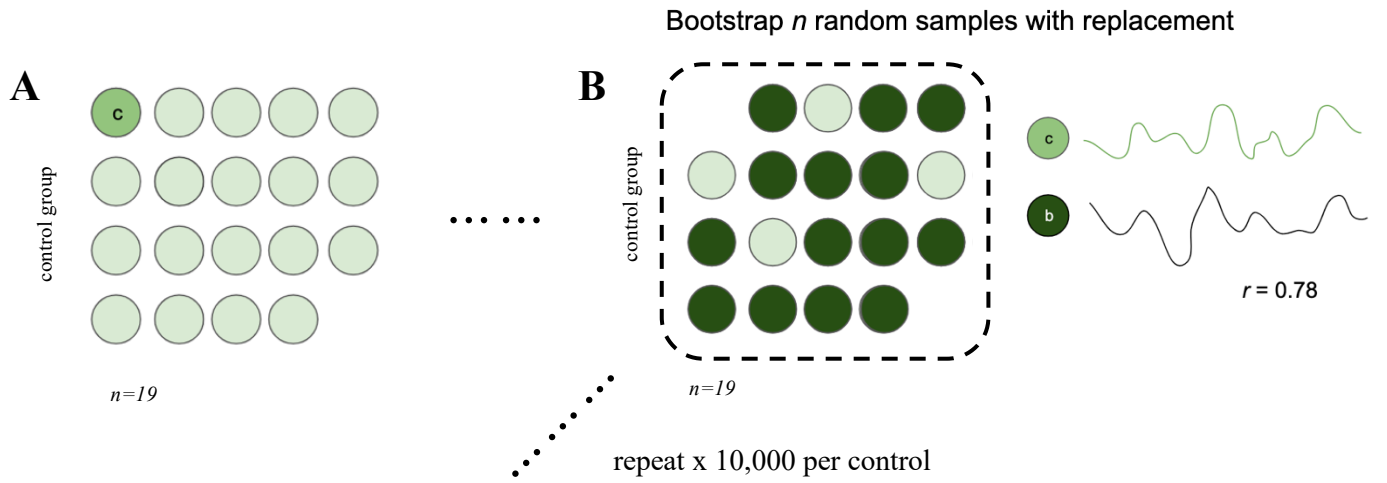


Figure 7. Schematic representation of the bootstrap correlation procedure for control subjects. First, a single control subject is selected and removed from the control group pool (A). The extracted white matter metrics across tracts of interest for this single control subject, represented as “c” are then correlated with the mean profile of a bootstrapped sample of size n , represented as “b” and a single correlation coefficient is obtained. This process is iteratively repeated 10,000 for each control, each time randomly selecting from the control pool with replacement in order to obtain a different control mean profile and r value (C). Note that the control “c” is never included in the bootstrapped mean profile “b” as they were first excluded from the control pool to reduce inflation of the correlation coefficient. Once all controls in the group have been bootstrapped, a histogram of the 190,000 computed correlation coefficients is constructed (D) and used to assess the probability of each patient’s correlation with the entire control group mean profile (E,F).

Chapter 3

3 Results

3.1 Behaviour Rating Inventory of Executive Functions

Age and gender standardized *t*-scores obtained using parental reports on the BRIEF2 revealed variable patient outcomes in four indices of executive dysfunction, including the Behaviour Regulation Index (BRI), Emotion Regulation Index (ERI), Cognitive Regulation Index (CRI) and the Global Executive Composite (GEC). *T*-scores within one standard deviation of 50 represented average ratings for neurotypically developing children, and the average *t*-scores for all controls in the current study fell within this expected normative range (Figure 8).

Patient 4A displayed mildly elevated *t*-scores on the ERI and typical scores on the remaining indices. One year later, as patient 4A2, the previously mildly elevated ERI *t*-score fell back within the expected range for children of the same age and gender. Patient 9A also displayed *t*-scores on all four indices of executive function within the expected range of neurotypically developing children and controls. Parental report revealed a potentially clinically elevated ERI for Patient 5A, and a mildly elevated GEC. The remaining patients 6A, 7A, 8A and 10A all displayed clinically elevated scores on the CRI, at least two standard deviations above the expected average. Patient 6A also scored in the potentially clinically elevated range on the BRI, and in the clinically elevated range on the GEC. In addition to clinically elevated CRI scores, patient 7A displayed clinically elevated ERI and GEC *t*-scores, and mildly elevated BRI scores. Patient 8A also displayed a clinically elevated GEC *t*-score and a mildly elevated ERI. Finally, patient 10A scored in the mildly elevated range on the BRI, and in the potentially clinically elevated range on the ERI and GEC. Overall, five out of the eight patients studied demonstrated *t*-scores at least in the potentially clinically elevated domain, and four of these patients reached clinically elevated scores in at least one of the four indices measured.

Behaviour Rating Inventory of Executive Functions (BRIEF2)

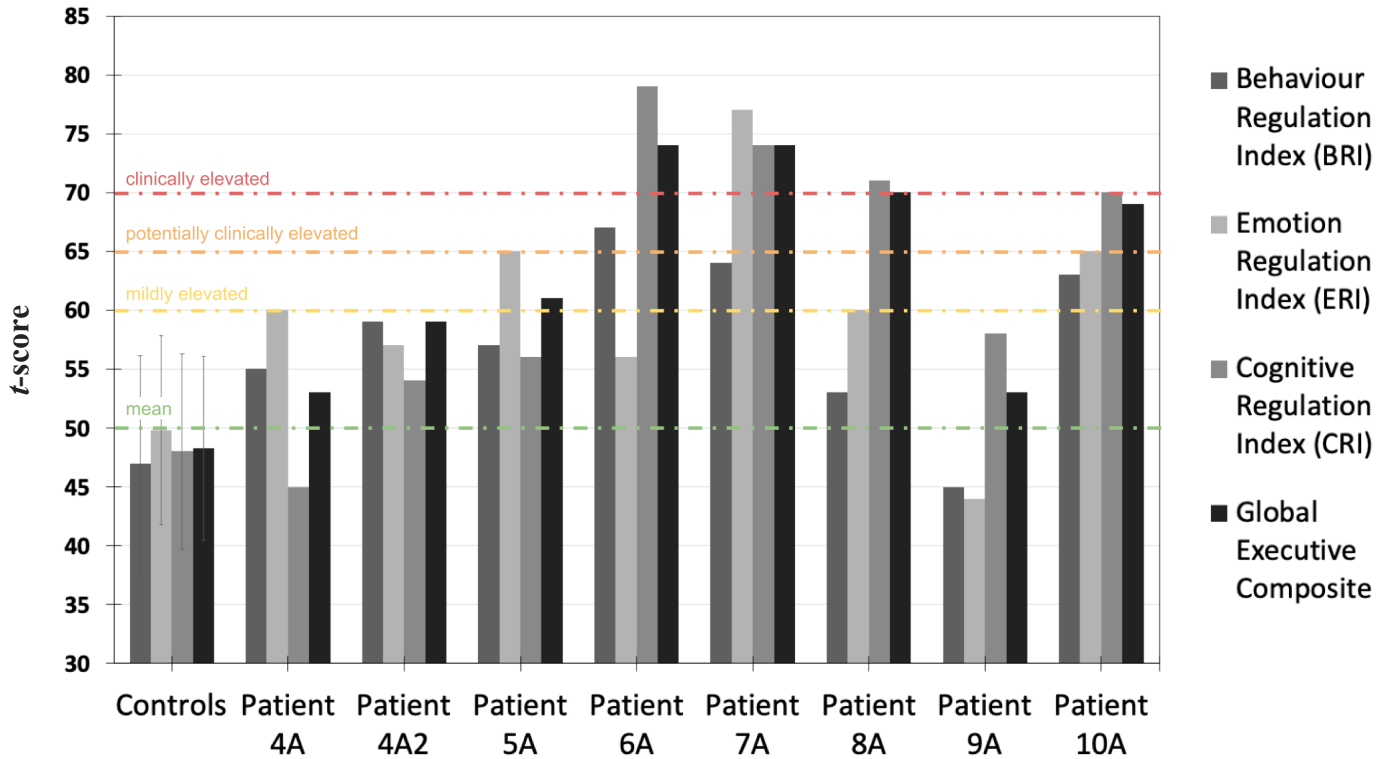


Figure 8. Age and gender standardized composite T scores of parental ratings on the Behaviour Rating Inventory for Executive Functions (BRIEF2). Patients with hydrocephalus are denoted with the letter 'A' and the mean t -scores for the control group are plotted with one SD . T -scores around 50 are indicative of average ratings for that age and gender. T -scores from 60 – 64 represent scores between 1 and 1.5 standard deviations above the mean, indicating mild executive dysfunction. T -scores from 65 – 69 represent scores between 1.5 and 2.0 standard deviations above the mean, indicating potentially clinical executive dysfunction. A t -score of 70 or above represents 2 standard deviations above the mean, which indicates clinical executive dysfunction. Parental reports for Patient 4A displayed average t -scores around the mean, except on the Emotion Regulation Index, which indicates mild elevation. Parental reports for patient 5A demonstrated mild elevation of scores on both the Emotion Regulation Index and the Global Executive Composite. Patients 6A, 7A and 8A scored in the clinically elevated range on the Global Executive Composite and patient 10A on the Cognitive Regulation Index. The control group mean was within 1 SD of the age and gender standardized mean for neurotypically developing children.

3.2 Striatal-Cortical Structural Connectivity

ROI-size corrected streamline counts obtained from probabilistic tractography were averaged across all children in the study and visualized as a 55x55 symmetric structural connectivity matrix (Figure 9A). For children in the control group, the 21 tracts that passed a weight-based connectivity threshold between the executive sub-region of the striatum and all 48 cortical ROIs were extracted and plotted as single mean structural connectivity vector with 95% confidence intervals. Regions displaying the highest structural connectivity with the executive striatum in controls included the frontal pole, inferior frontal gyrus, frontal orbital cortex, frontal operculum cortex and insular cortex. Individual connectivity vectors representing single patients were then plotted along with the control group mean profile. Visual inspection revealed that most patients displayed higher than average structural connectivity with the frontal pole, however lower than average connectivity with the inferior frontal gyrus. Correlations with the control group mean profile revealed significant dissimilarity for patients 7A, 9A, 4A and 5A when compared to a bootstrapped distribution of control correlations (Figure 11A; $r = .67, .68, .75, \text{ and } .77$, respectively; $p < .001$). Patients 8A, 4A2, and 2A all showed executive striatal-cortical structural connectivity profiles similar to the control group mean profile when placed in the same bootstrapped correlation distribution ($r = .86, .86, .93, p > .01$).

3.3 Striatal-Executive Network White Matter Integrity

White matter integrity was assessed in the same 21 striatal-executive tract volumes which passed the weight-based connectivity threshold reported above. The same approach for visualizing FA, MD, AD, RD and MTR across these tracts was taken as well; the control group mean profile was plotted with 95% confidence intervals with individual patient profiles plotted alongside (Figure 10).

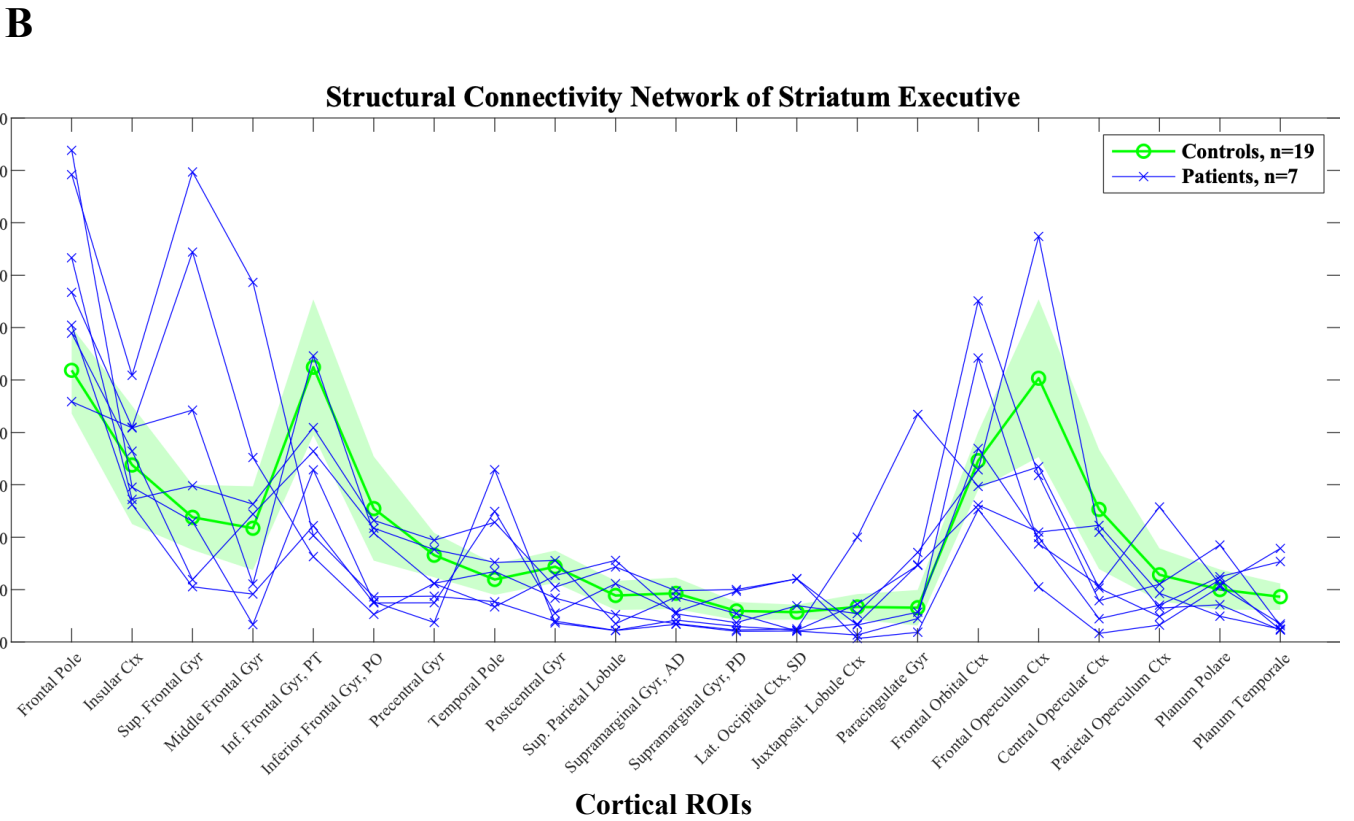
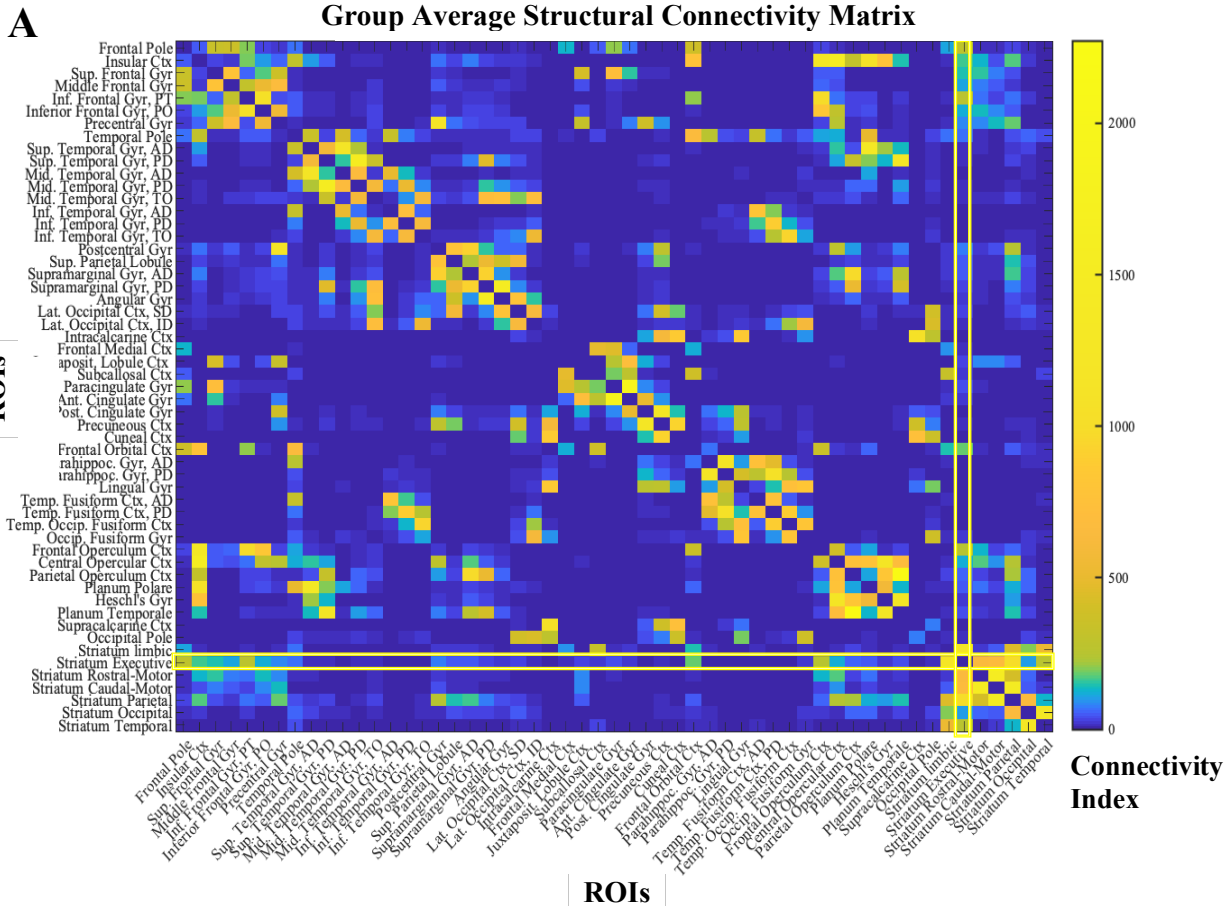


Figure 9. (A) A symmetrical 55x55 structural connectivity matrix containing ROI-size corrected streamline counts, averaged across all controls and patients in the study. The color map represents the value of the connectivity index, with darker blues reflecting lower structural connectivity and yellows reflecting higher structural connectivity. The highlighted yellow column/row represents the tracts in the Striatum Executive network used for analysis. (B) A structural connectivity vector of corrected streamline counts, containing tracts between the striatum executive sub-region and 21 cortical targets passing a weight-based threshold. The mean profile across healthy controls ($n=19$) is displayed in green with 95% confidence intervals and individual patients with hydrocephalus ($n=7$) are displayed in blue.

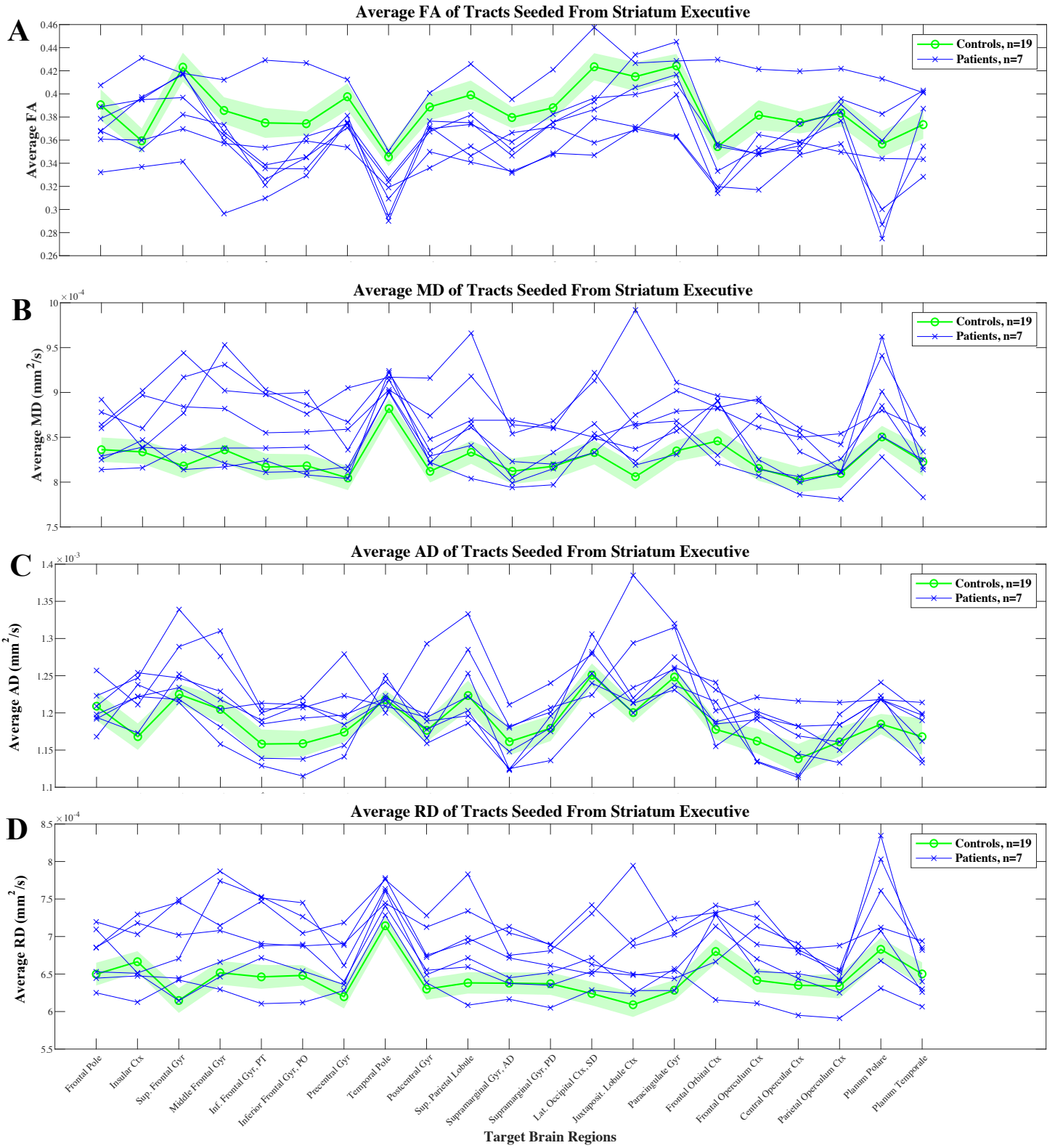
Visual inspection of the average FA values within striatal-executive tract volumes in patients revealed a trend of lower values when compared to the control group mean, however one patient had consistently higher FA across tracts (Figure 10A) Apart from this one patient, FA values were consistently below the control average in tracts connecting the executive striatum with frontal regions such as the superior frontal gyrus, middle frontal gyrus, and inferior frontal gyrus. Correlations with the control group mean profile revealed significant dissimilarity of FA profiles for patients 7A, 4A2, and 8A, when compared to a bootstrapped distribution of control correlations (Figure 11B; $r=.47$ and $.58$, respectively; $p<.01$). Patients 2A, 5A, 4A, and 9A's FA profiles highly correlated with the control group mean and placed within the expected distribution obtained from the control bootstrap procedure ($r=.70$, $.70$, $.71$ and $.78$, respectively; $p>.01$).

Patients demonstrated a trend of higher MD profiles when visually inspected across all 21 striatal executive tracts and compared to the control group mean profile, although some patients fell within the 95% confidence intervals of the control mean (Figure 10B). Correlations with the control group mean profile revealed that patients 5A, 9A, 2A, and 8A, were significantly uncorrelated when compared to the bootstrapped distribution of control correlations (Figure 11C; $r=.20$, $.45$, $.51$, and $.62$, respectively; $p<.01$). Patients 7A, 4A2 and 4A were significantly correlated with the control group mean when compared to the bootstrapped distribution ($r=.70$, $.85$, and $.88$, respectively; $p>.01$).

Visual inspection of the average AD patient profiles demonstrated both higher and lower scores when compared to the control group mean, depending on the tract (Figure 10C). Patient 5A's AD profile was significantly dissimilar when correlated with the control group mean and compared to the bootstrapped correlations obtained from the controls (Figure 11D; $r = .59$; $p < .01$). Patient 2A, 9A, 4A, 7A, 4A2, and 8A's AD profiles were correlated with the control group mean within the expected distribution obtained from the control bootstrap procedure ($r = .67, .69, .70, .72, .74$ and $.76$, respectively; $p > .01$).

Average RD values within the isolated striatal executive network were also visually inspected for all patients and compared to the control group mean profile. Across most tracts, including those connecting the executive sub-region of the striatum with the superior frontal gyrus, inferior frontal gyrus, and temporal pole, patients had higher RD values than the control group average (Figure 10D). However, one patient showed consistently lower RD across tracts. When assessing the similarity of patient profiles with the control group mean profile in bootstrapped distribution of control correlations, patients 5A, 7A, 8A, 2A and 9A had significantly uncorrelated RD values within this striatal executive network (Figure 11E; $r = .26, .45, .48, .52$, and $.57$, respectively; $p < .01$). Patient 4A/4A2 however displayed RD profiles which were correlated to the control group mean profile according to the bootstrap analysis ($r = .85$ and $.72$, respectively; $p > .01$).

Finally, visual inspection of MTR values within the same striatal executive network demonstrated that patients fell within the 95% confidence intervals of the control group average for most tracts (Figure 10E). The exceptions were tracts connecting the executive striatum with the temporal pole, lateral occipital cortex, and paracingulate gyrus. Correlations of patient MTR values with the control group mean profile revealed that patients 9A had significant dissimilarity when compared to the bootstrapped control correlations (Figure 11F; $r = .61$; $p < .01$). However, patients 7A and 8A were not significantly dissimilar from the control group mean profile when tested within the same bootstrapped distribution ($r = .74$ and $.66$, respectively; $p > .01$).



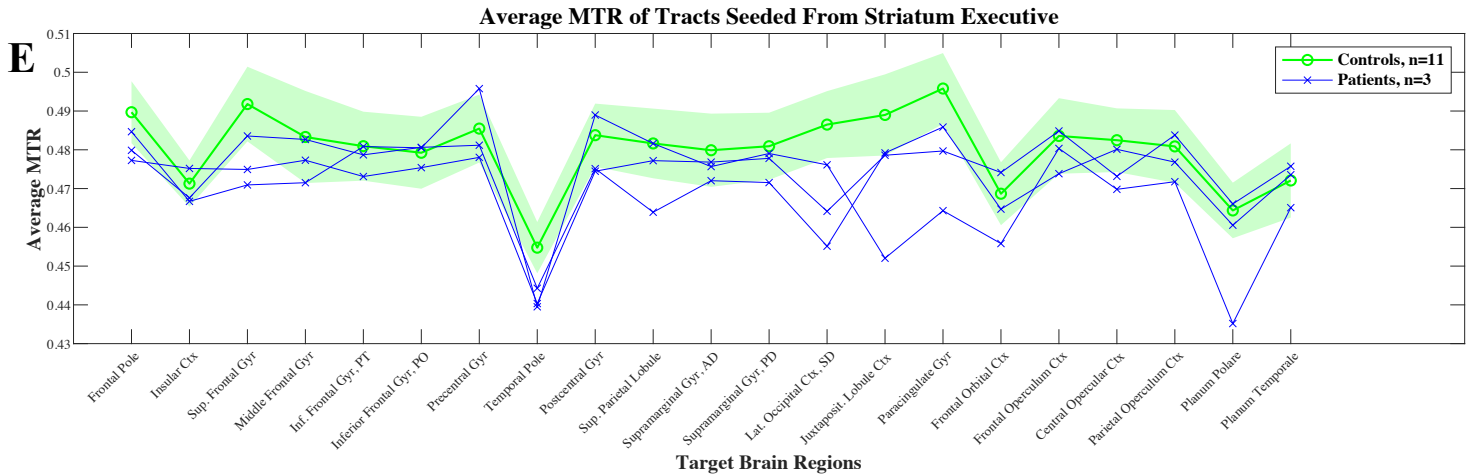


Figure 10. (A) The average fractional anisotropy (FA) in tracts seeded from the executive sub-region of the striatum is plotted for individual patients ($n=7$) in blue, and the control group mean profile is represented in green with 95% confidence intervals ($n=19$). The same visualization approach was used to assess (B) mean diffusivity (MD); (C) axial diffusivity (AD); (D) radial diffusivity (RD); and (E) the magnetization transfer ratio (MTR). There were less controls ($n= 11$) and patients ($n=3$) that were able to complete the MTR protocol as it was at the end of an hour-long imaging protocol.

3.4 FA Linear Regression with GEC

A linear regression was performed to assess the relationship between GEC t -scores and striatal-executive network FA correlations with the control mean profile. Higher GEC values reflect higher degrees of executive dysfunction. Lower correlation coefficients of FA with the control mean profile represents higher dissimilarity across the network. Our regression revealed a significant negative linear relationship between the FA dissimilarity in the striatal executive network and GEC t -scores (Figure 12A; $R^2=.728$, $F_{1,4}= 10.7$, $p<.05$). To assess whether this relationship was specific to the striatal executive network, an additional regression investigating FA-correlations in the striatal-occipital network and GEC t -scores was performed. The results demonstrated that correlations of the striatal occipital network did not significantly explain variability in patient GEC t -scores (Figure 12B, $R^2=.097$, $F_{1,4}= 0.431$, $p=.547$).

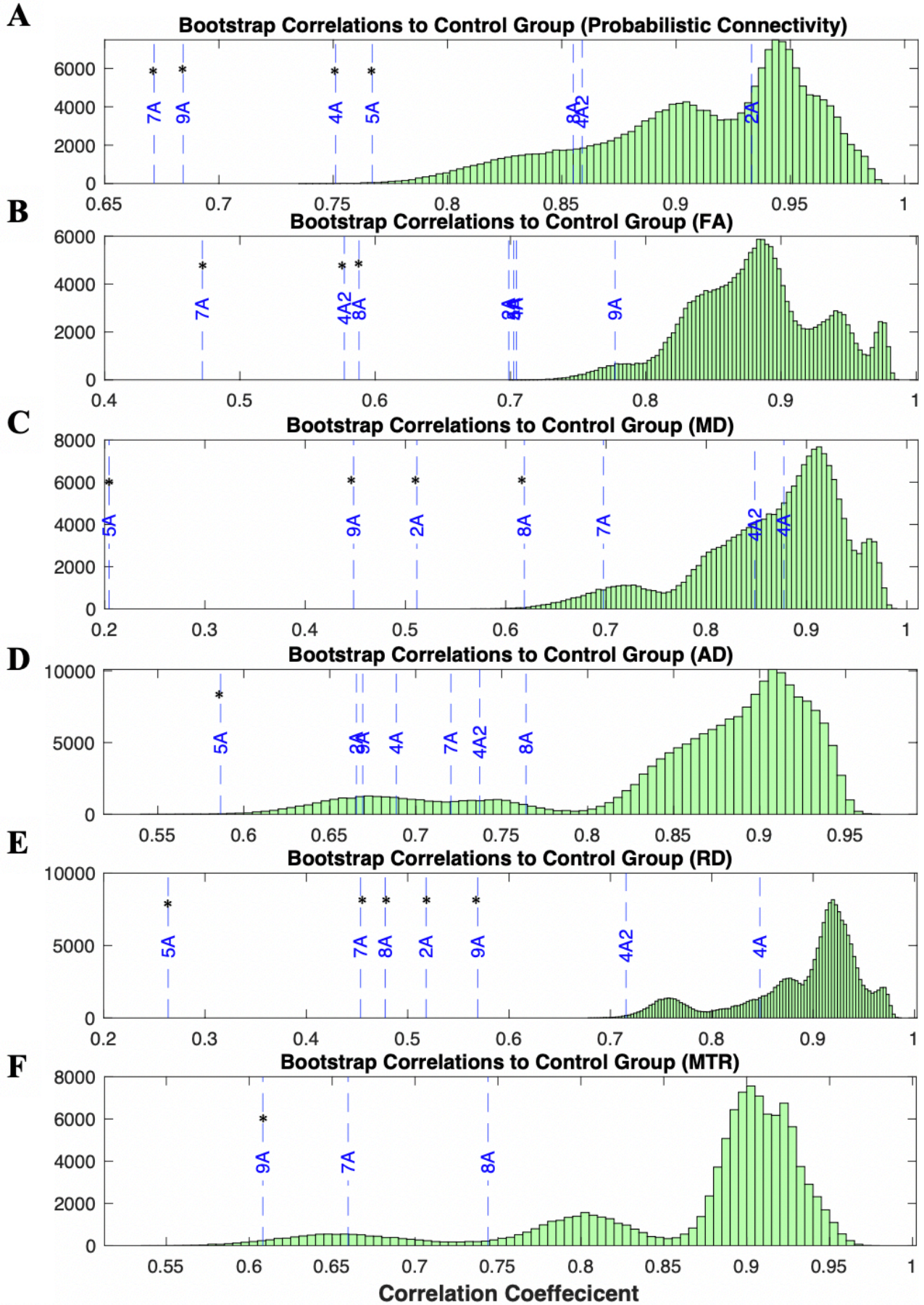


Figure 11. (A) Control fractional anisotropy (FA) profiles across the striatal-executive network, were bootstrap correlated with randomly sampled control group mean profiles to obtain a distribution of correlation coefficients (10,000 correlations computed for each control; green). Patient fractional anisotropy (FA) profiles were correlated with the control group mean profile and plotted within the bootstrapped distribution (blue). Asterisks (*) denote patients falling outside of the control bootstrap distribution with $p < .01$. The same steps were taken for profiles of MD (B), AD (C), RD (D) and MTR (E).

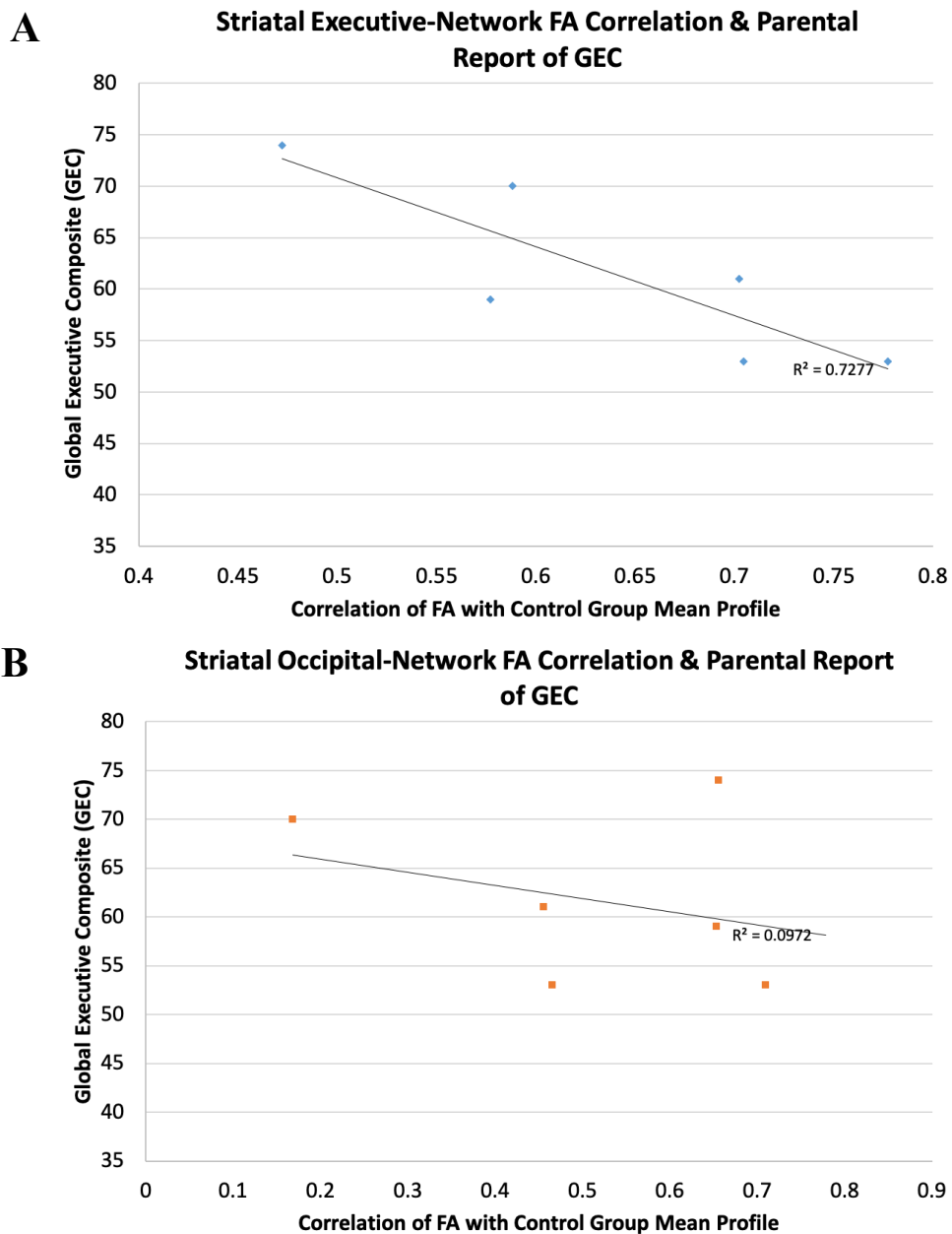


Figure 12. (A) A negative linear relationship was found between FA-correlations with the control mean profile in the striatal-executive network and the Global Executive Composite (GEC) scores across patients with hydrocephalus ($R^2=.728$, $F_{1,4}= 10.7$, $p<.05$). (B) FA-correlations of the striatal-occipital network were not able to significantly explain variability in the same GEC scores across patients ($R^2=.097$, $F_{1,4}= 0.431$, $p=.547$).

Chapter 4

4 Discussion

The current pilot study aimed to investigate changes in striatal white matter integrity and connectivity in a small sample of school-aged children with shunted hydrocephalus, years after their initial diagnosis and treatment. It was hypothesized that ventricular dilatation due to hydrocephalus in infancy could impair the development of higher-order cognitive functions and that white matter status within the striatal-executive network would reflect the severity of executive dysfunction. Using a behavioural MRI approach, patients were recruited to undergo a diffusion-weighted neuroimaging protocol while parental reports of executive function were simultaneously obtained. Probabilistic tractography was used to reconstruct sub-regionally specific striatal structural networks in native diffusion space, which was then used to assess structural connectivity and also diffusivity within tract volumes. Departures from an age-matched control mean profile, obtained by averaging 19 control children on measures of structural connectivity, FA, MD, AD, RD and MTR were visually inspected across patients. The bootstrap method was employed to test the similarity of individual patient networks with controls on all the above metrics by computing correlations with the control mean profile. Lower correlation coefficients represented higher dissimilarity from the control mean profile. One aim of this study was to identify how changes in white matter reflected the development status of higher-order neurocognitive functions, known as executive functions. A linear regression was therefore performed to identify how changes in FA-correlations within the striatal-executive network accounted for variability in GEC *t*-scores, and the specificity of this finding was explored by also performing a regression with the FA-correlations of the striatal-occipital network.

4.1 Executive Dysfunction

Results from parental reports on the BRIEF2 revealed variable outcome, with patients such as 4A2 and 9A falling within the expected values of the normative reference sample on all indices of executive function, and other patients such as 6A, 7A, 8A and 10A reaching clinically elevated scores on the CRI. Overall, evidence of executive dysfunction obtained

from the 4 composite scores was found in variable degrees across patients. A previous study by Mahone, Zabel, Levey, Verda and Kinsman (2002) using an older version of the BRIEF in adolescents with spina bifida and hydrocephalus found that parents reported more problems on the Global Executive Composite of the BRIEF than on the three common indices of the Behavior Assessment System for Children (BASC; Reynolds & Kamphaus, 1998a, 1998b). Interestingly, the adolescents with hydrocephalus in their study were also more likely to self-report executive dysfunction in the Behavioural Regulation Index, while their parents reported lower scores on the Metacognitive Index. While the nature of executive dysfunction is likely to be mediated based on factors such as etiology, whether there is a form of dysfunction that is more vulnerable than others to ventricular dilatation and high ICP remains to be explored. Future work with larger patient samples and higher power can also investigate the individual clinical scales derived from the BRIEF shown in Figure 2 as means of disentangling underlying deficits contributing to GEC scores.

Although the current thesis only reported findings pertaining to parental reports on the BRIEF2, all patients and controls were also tested on performance-based measures using a mobile touchscreen battery. The testing battery was designed in-house and was used to obtain a multitude of performance metrics reflecting the various domains of executive functioning through computerized tasks in the form of games, which were designed to engage children while being easy to administer. The tasks included:

1. A size-congruency task which requires selecting the numerically larger value of two options that differ in physical size.
2. A digit span task that requires the participant to recall an increasingly lengthier series of numbers.
3. A visual-spatial working memory task that requires remembering a sequence of objects and their respective locations.
4. A working memory task that involves counting bags that go into an x-ray scanner and reporting how many are missing.

5. A 2D manipulation task that involves mental rotation of an object and identification among 4 different options.
6. An intra-dimensional and extra-dimensional shift task that requires cognitive flexibility and adapting to new rules for correct responses.
7. A spatial reasoning task that involves counting the least number of moves required to match the blocks on two trees.
8. A go/no-go whack-a-mole task that involves quickly selecting moles as they appear and avoiding moles that are wearing a hat.

These tasks were developed to assess various domains of executive function, including selective attention, attention shifting and flexibility, working memory, planning, and response inhibition. However, validation with other performance-based measures or golden standards such as the BRIEF, is one possible future direction. As performance-based measures can assess a wide variety of specific executive functions, future work can potentially identify if a specific underlying cognitive deficit is driving the dysfunction being reported by parents.

4.2 The Striatal Executive Network

Our results from probabilistic tractography revealed that structural connectivity within the striatal-executive network was significantly dissimilar from the healthy control profile. Specifically, patients 7A, 9A, 4A and 5A all exhibited lower correlations with the control mean when compared to the bootstrapped distribution of control correlations. These findings could reflect the impact of ventricular dilatation on white matter fibers and the re-organization of neural circuitry post-injury. Indeed, a previous study investigating structural networks using DTI in pediatric patients suffering from traumatic brain injury revealed altered network topology, characterized by hyper-connectivity of “rich club” nodes (which are the network cores marked by high degree nodes) relative to healthy controls, at the expense of local connectivity (Dennis et al., 2017). Although our study did not inspect the

entire structural connectivity matrix using graph theoretical analysis, our analysis specific to the striatal-executive network was still sensitive to aberrant connectivity in patients when compared to controls. Decreased correlations with the control mean could reflect both hyper-connectivity and hypo-connectivity across nodes in the network due to brain injury at young age. Interestingly, upon visual inspection of the corrected structural connectivity index in Figure 9B, patients tended to demonstrate higher levels of connectivity with the frontal pole than the control average, which possibly reflects this “rich club” hyper-connectivity phenotype, although further investigation is required to fully characterize the striatal network topology in our sample .

Other studies assessing both functional MRI and DTI in infants with IVH and post-hemorrhagic hydrocephalus have also found aberrant changes in resting-state networks, with some infants demonstrating increases in both structural and functional connectivity in the weeks before and after VP shunt placement (Smyser et al, 2013; Smyser 2019). Furthermore, preterm infants with periventricular leukomalacia, a neurological condition primarily impacting white matter, also shown re-organization of frontal-striatal and frontal-limbic white matter pathways when compared to healthy children (Ceschin, Lee, Schmithorst, & Panigraphy, 2015). These changes in network connectivity could thus reflect the plastic brain’s attempt to re-organize neural circuitry following white matter damage due to ventricular dilatation.

In addition to aberrant structural connectivity, changes in white matter integrity measured using DTI and MTR were also found in corticostriatal tracts. Our results revealed every single patient except 4A showed significantly lower correlations to the control profile on at least one metric of white matter integrity, ranging from FA, MD, AD, RD and MTR, corrected for multiple comparisons. Specifically, the striatal-executive profiles measuring MD and RD captured the highest proportions of patients with significantly lower correlations to the control group mean (Figure 11 C, E). Visual inspection revealed that most patients showed higher MD and RD values in the executive-striatum network in reference to the control group mean (Figure 10 B, D). Higher levels of MD and RD and disproportionate increases across the striatal network when compared to healthy controls likely contributed to lower correlations. Furthermore, high RD reflects an increase in diffusion which is

perpendicular to the principal diffusivity vector (Figure 3) and is possibly the result of impaired myelination of axonal membranes across neurodevelopment. One study which used a cuprizone mouse model of demyelination showed that changes in myelination assessed using immunostaining techniques reflected changes in RD in the corpus callosum, and that RD values were specific to the time course of changes in myelin integrity and distinct from acute axonal injury (Song et al., 2005). Other studies have noted damage to white matter in pediatric hydrocephalus which persists after shunt placement, and that apoptosis of oligodendrocytes responsible for myelinating the brain could be a driving factor for observed RD increases (Air et al., 2010; Assaf et al., 2006; Isaacs et al., 2019; Mangano et al., 2016; Scheel, Diekhoff, Sprung, & Hoffmann, 2012; Ludwin, 1980). Thus, it is likely that patients in our study showing significantly lower correlations of RD have underlying differences in myelination status, and that alterations in other metrics like MD and FA also reflect similar states of lower white matter integrity.

Patient 4A was the only patient similar to control profiles on all measured diffusivity metrics (FA, MD, AD, and RD; Figure 11B-E), however one year later as patient 4A2 their striatal-executive network FA was significantly less correlated with the control mean profile. Although it is not entirely clear what this result reflects, it could be that differences from a typical profile begin to emerge or become more apparent later in development as the healthy counterparts continually myelinate striatal-executive tracts. If a patient had regionally aberrant myelination patterns within a network, this could result in a lower FA correlation with the control mean profile. Although not significant due to our correction for multiple comparisons, patient 4A2 was also trending towards lower correlation with the RD mean profile, a potential sign of impaired myelination status. Nonetheless, future longitudinal work in developing patient and healthy control samples or experimental animal models would be better posed to assess this question.

Although our sample size was diminished for the MTR protocol, as it was at the end of our entire 1hr 15 min imaging series, we were still able to assess 3 patients and 11 controls. In particular, Patient 9A's striatal-executive network showed significantly lower MTR correlations within the bootstrapped distribution, and patients 7A and 8A were not significantly different from controls. MTR is a marker for macromolecules such as the lipid-

content in white matter, and lower levels are associated with decreases in myelination. While our correlation-approach is not specific to decreases in MTR, but rather any deviations from the control mean profile, it is still possible that lower MTR in a number of tracts within the network drives a reduced correlation. Furthermore, visual inspection of patient 9A's MTR profile revealed lower MTR in tracts connecting with the juxtapositional lobule cortex (supplementary motor area), paracingulate gyrus, and planum polare than the control profile. These regions are highly connected with the frontal cortex, known to play roles in coordinating locomotion, allocating attention and language.

When investigating FA within the striatal-executive network, patients 7A, 4A2 and 8A showed significantly lower correlations to the control profile (Figure 11B). Lower FA values across ROIs in patient networks were present when compared to controls, which potentially reflects decreases in white matter integrity due to ventricular dilatation. In one study of children with ADHD, reduction of FA in fronto-striatal tracts significantly correlated with symptom severity and executive functioning performance on the Cambridge Neuropsychological Test Automated Battery (Shang, Wu, Gau & Tseng, 2013). In our study we were also interested in assessing whether differences in white matter integrity measured by FA correlated with differences in GEC *t*-scores. Damage to periventricular white matter structures, such as the corpus callosum, fornix and internal capsule, has been consistently reported to be a major factor associated with poor neurological outcome, including decreases in performance IQ scores and motor, visuo-spatial and language skills (Fletcher et al., 1992; Fletcher et al., 1996; Hannay, 2000). However, impairments in the development of higher-order function later in childhood and the related integrity of striatal tracts has yet to be investigated using DTI.

In order to test this function-structure relationship, we performed a regression analysis on the FA correlation co-efficients and GEC *t*-scores obtained from the BRIEF (Figure 12A). We found a significant negative linear relationship in our sample of patients, meaning that higher executive dysfunction measured by the GEC was related to lower FA correlations in the striatal-executive network to healthy controls. To test whether lower executive dysfunction was related to another striatal network that has a high susceptibility to damage, we performed another regression on GEC scores, except this time with the FA of striatal-occipital network

(Figure 12B). The results were not significant, meaning that variability in the patient GEC scores was not related to differences in FA correlations of tracts travelling towards more posterior brain regions. Even though ventricular dilatation progresses into both posterior-anterior white matter, impairment of global executive function was only related to damage in the striatal-executive network. Although our small patient sample may or may not be contributing to this finding, it is specific to tracts expected to play a role in the development of executive function. Greater white matter changes and alterations occurring within this striatal-executive network due to ventricular dilation could thus be one important predictor of executive functioning outcome.

4.3 Caveats & Limitations

With only 7 patients in our current study, the scope of our white matter analysis was limited to identifying how each individual patient related to the controls DTI metrics and MTR. We were also only able to identify how individual patients compared to normative reference data in terms of executive functioning outcome and we were not able to perform an appropriately powered group-analysis. While we did implement a bootstrapping method that was sensitive to alterations of the striatal-executive network between individual patients and controls, our small sample limits the generalizability of our findings to children presently included in this study. Nonetheless, small samples in clinical pediatric research are relatively common and have still provided valuable insight into possible mechanisms impacting neurodevelopment across scientific history.

Furthermore, while the current pilot study was too under-powered to investigate the relationship of etiology with executive functioning outcomes and structural integrity, it is important to keep in mind that etiological differences do exist among these children that contribute to observed cognitive and neuropsychological deficits (Fletcher et al., 2000). Other factors which were not included in the present analysis, such as age of onset, number of revisions, prematurity, and birthweight, likely play a role in developmental outcome as well. While the current study was not able to appropriately test these variables, future research with larger samples can identify their unique relationships with DTI-related metrics using a multiple regression approach.

Additionally, although our patients were age-matched with the control group, they ranged from 6-10 years old, and possible developmental changes in striatal-executive white matter could thus be captured by our measures. Future longitudinal work with larger samples could thus investigate age-specific differences in patients with hydrocephalus and healthy controls, and whether deviation from a neurotypical can become more apparent later in development for certain patients.

One aspect of the current study that can be revisited in the future was our approach to isolating regionally specific striatal networks. In the current investigation, we defined our network based on the values of corrected streamline counts, such that only tracts containing streamlines above 10% of the maximum count would be included. However, studies have shown this weight-based approach can be biased towards selecting for streamlines that travel shorter distances, while consistency-based thresholds derived from a coefficient of variation (CV) can resolve this issue (Roberts, Perry, Roberts, Mitchell & Breakspear, 2017). The CV of every tract can be computed by dividing the standard deviation by its mean value across subjects. Tracts with lower CVs are more consistent in the group. By selecting for tracts that show lower variance across all ROIs for the entire group, tracts that tend to be strong for their length are included in the network rather than tracts that tend to shorter. However, studies implementing this approach have been done in adults, and one question as to how this consistency-based approach reduces developmental-related variability in the resulting network still remains. I therefore opted to avoid implementing this consistency-based threshold in our pediatric sample, with the risk of biasing networks to include tracts of shorter streamlines. One possible alternative is to include variability of streamline length in our calculation of the corrected connectivity index, as a means to assess the weight of connections independent of length.

4.4 Conclusions

The current pilot study using DTI and MTR to investigate white matter outcomes in a small sample of school aged children with VP shunted hydrocephalus was able to highlight deviations in striatal structural connectivity and integrity when compared to age-matched healthy controls. Using a bootstrap resampling technique to construct distributions of control

correlation co-efficients, highlighting that small sample studies can still be sensitive and capture individual patient deviations from a typical structural profile. Lower patient correlations of RD and MD was interpreted as a possible marker of impaired myelination due to early life ventricular dilatation; however, more research is needed to fully characterize developmental differences in patients. The patients in the current study also demonstrated variable executive functioning outcome obtained by parental reports on the BRIEF2, with a number of patients reaching clinically elevated dysfunction across the ERI, BRI, CRI and GEC, whereas others were within the expected range for children of their age and gender. Variability in outcome could be related to a number of different factors which the current study was unable to explore. Furthermore, a structure-function relationship of striatal-executive FA and executive functioning outcome was detected in patients. Patients with higher executive dysfunction measured by the GEC also had lower correlation of FA with the healthy control profile, linking the importance of white matter sub-regionally specific striatal circuitry. Overall, a more robust understanding of the impacts of early life ventricular dilation on white matter and higher-order cognitive outcome can help parents and neurosurgeons make clinical decisions in the course of treatment, better understand an infant's prognosis and access appropriate interventions. Future work with larger samples and consortium-style studies could help test the generalizability of these results to the larger patient population, while also investigating how etiology, prematurity, ICP, and revisions impact striatal tracts and neurodevelopmental outcomes.

References

- Air, E. L., Yuan, W., Holland, S. K., Jones, B. V., Bierbrauer, K., Altaye, M., & Mangano, F. T. (2010). Longitudinal comparison of pre-and postoperative diffusion tensor imaging parameters in young children with hydrocephalus. *Journal of Neurosurgery: Pediatrics*, 5(4), 385-391.
- Alvarez, J. A., & Emory, E. (2006). Executive function and the frontal lobes: a meta-analytic review. *Neuropsychology review*, 16(1), 17-42.
- Assaf, Y., Ben-Sira, L., Constantini, S., Chang, L. C., & Beni-Adani, L. (2006). Diffusion tensor imaging in hydrocephalus: initial experience. *American journal of neuroradiology*, 27(8), 1717-1724.
- Bagnato, F., & Frank, J. A. (2003). The role of nonconventional magnetic resonance imaging techniques in demyelinating disorders. *Current neurology and neuroscience reports*, 3(3), 238-245.
- Bammer, R., Acar, B., & Moseley, M. E. (2003). In vivo MR tractography using diffusion imaging. *European journal of radiology*, 45(3), 223-234.
- Behjati, S., Emami-Naeini, P., Nejat, F., & el Khashab, M. (2011). Incidence of hydrocephalus and the need to ventriculoperitoneal shunting in premature infants with intraventricular hemorrhage: Risk factors and outcome. *Child 's Nervous System*, 27(6), 985–989
- Behrens, T. E., Berg, H. J., Jbabdi, S., Rushworth, M. F., & Woolrich, M. W. (2007). Probabilistic diffusion tractography with multiple fibre orientations: What can we gain?. *Neuroimage*, 34(1), 144-155.
- Behrens, T. E., Woolrich, M. W., Jenkinson, M., Johansen-Berg, H., Nunes, R. G., Clare, S., ... & Smith, S. M. (2003). Characterization and propagation of uncertainty in diffusion-weighted MR imaging. *Magnetic Resonance in Medicine: An Official Journal of the International Society for Magnetic Resonance in Medicine*, 50(5), 1077-1088.

- Benavente-Fernández, I., Synnes, A., Grunau, R. E., Chau, V., Ramraj, C., Glass, T., ... & Miller, S. P. (2019). Association of socioeconomic status and brain injury with neurodevelopmental outcomes of very preterm children. *JAMA network open*, *2*(5), e192914-e192914.
- Bigler, E. D. (1988). The neuropsychology of hydrocephalus. *Archives of Clinical Neuropsychology*, *3*, 81–100.
- Brewer, V. R., Fletcher, J. M., Hiscock, M., & Davidson, K. C. (2001). Attention processes in children with shunted hydrocephalus versus attention deficit hyperactivity disorder. *Neuropsychology*, *15*(2), 185–198.
- Briggs, F., & Usrey, W. M. (2008). Emerging views of corticothalamic function. *Current opinion in neurobiology*, *18*(4), 403-407.
- Brookshire, B. L., Fletcher, J. M., Bohan, T. P., Landry, S. H., Davidson, K. C., & Francis, D. J. (1995). Verbal and nonverbal skill discrepancies in children with hydrocephalus: a five-year longitudinal follow-up. *Journal of Pediatric Psychology*, *20*(6), 785-800.
- Burmeister, R., Hannay, H. J., Copeland, K., Fletcher, J. M., Boudousquie, A., & Dennis, M. (2005). Attention problems and executive functions in children with spina bifida and hydrocephalus. *Child Neuropsychology*, *11*(3), 265-283.
- Bystron, I., Blakemore, C., & Rakic, P. (2008). Development of the human cerebral cortex: Boulder Committee revisited. *Nature Reviews Neuroscience*, *9*(2), 110.
- Casey, B. J., Giedd, J. N., & Thomas, K. M. (2000). Structural and functional brain development and its relation to cognitive development. *Biological psychology*, *54*(1-3), 241-257.
- Catalão, C. H. R., Correa, D. A. L., Garcia, C. A. B., Dos Santos, A. C., Salmon, C. E. G., Rocha, M. J. A., & da Silva Lopes, L. (2014). Pre-and postshunting magnetization transfer ratios are in accordance with neurological and behavioral changes in hydrocephalic immature rats. *Developmental neuroscience*, *36*(6), 520-531.

- Ceschin, R., Lee, V. K., Schmithorst, V., & Panigrahy, A. (2015). Regional vulnerability of longitudinal cortical association connectivity: associated with structural network topology alterations in preterm children with cerebral palsy. *NeuroImage: Clinical*, 9, 322-337.
- Cheng, H., Wang, Y., Sheng, J., Kronenberger, W. G., Mathews, V. P., Hummer, T. A., & Saykin, A. J. (2012). Characteristics and variability of structural networks derived from diffusion tensor imaging. *Neuroimage*, 61(4), 1153-1164.
- Chern, J. J., Muhleman, M., Tubbs, R. S., Miller, J. H., Johnston, J. M., Wellons, J. C., ... & Rozzelle, C. J. (2012). Clinical evaluation and surveillance imaging in children with spina bifida aperta and shunt-treated hydrocephalus. *Journal of Neurosurgery: Pediatrics*, 9(6), 621-626.
- Chumas, P. D., Drake, J. M., Del Bigio, M. R., Da Silva, M., & Tuor, U. I. (1994). Anaerobic glycolysis preceding white-matter destruction in experimental neonatal hydrocephalus. *Journal of neurosurgery*, 80(3), 491-501.
- Cole, M. W., & Schneider, W. (2007). The cognitive control network: integrated cortical regions with dissociable functions. *Neuroimage*, 37(1), 343-360.
- Cools, R., & D'Esposito, M. (2011). Inverted-U-shaped dopamine actions on human working memory and cognitive control. *Biological psychiatry*, 69(12), e113-e125.
- Crespy, L., Zaaraoui, W., Lemaire, M., Rico, A., Faivre, A., Reuter, F., Malikova, I., Confort-Gouny, S., Cozzone, P. J., Pelletier, J., Ranjeva, J. P., & Audoin, B. (2011). Prevalence of grey matter pathology in early multiple sclerosis assessed by magnetization transfer ratio imaging. *PloS one*, 6(9), e24969.
- Croxson, P. L., Johansen-Berg, H., Behrens, T. E., Robson, M. D., Pinsk, M. A., Gross, C. G., ... & Rushworth, M. F. (2005). Quantitative investigation of connections of the prefrontal cortex in the human and macaque using probabilistic diffusion tractography. *Journal of Neuroscience*, 25(39), 8854-8866.
- Dandy, W. E. (1919). Experimental hydrocephalus. *Annals of surgery*, 70(2), 129.

- Dandy, W. E., & Blackfan, H. D. (1914). An Experimental and Clinical Study of Internal Hydrocephalus, *J. AMA* 61: 2216 (Dec. 20) 1913; Internal Hydrocephalus: An Experimental, Clinical and Pathological Study. *Am. J. Dis. Child*, 8, 406.
- de Reus, M. A., & van den Heuvel, M. P. (2013). Estimating false positives and negatives in brain networks. *Neuroimage*, 70, 402-409.
- Del Bigio, M. R., da Silva, M. C., Drake, J. M., & Tuor, U. I. (1994). Acute and chronic cerebral white matter damage in neonatal hydrocephalus. *Canadian Journal of Neurological Sciences*, 21(4), 299-305.
- Del Bigio, M. R., Kanfer, J. N., & Zhang, Y. W. (1997). Myelination delay in the cerebral white matter of immature rats with kaolin-induced hydrocephalus is reversible. *Journal of Neuropathology & Experimental Neurology*, 56(9), 1053-1066.
- Del Bigio, M. R. (1989). Hydrocephalus-induced changes in the composition of cerebrospinal fluid. *Neurosurgery*, 25(3), 416-423.
- Del Bigio, M. R. (2000). Calcium-mediated proteolytic damage in white matter of hydrocephalic rats? *Journal of Neuropathology & Experimental Neurology*, 59(11), 946-9
- Del Bigio, M. R. (2010). Neuropathology and structural changes in hydrocephalus. *Developmental disabilities research reviews*, 16(1), 16-22.
- Dennis, E. L., Rashid, F., Babikian, T., Mink, R., Babbitt, C., Johnson, J., ... & Thompson, P. M. (2017). Altered network topology in pediatric traumatic brain injury. In *13th International Conference on Medical Information Processing and Analysis* (Vol. 10572, p. 105720P). International Society for Optics and Photonics.
- Domínguez-Pinos, M. D., Páez, P., Jiménez, A. J., Weil, B., Arráez, M. A., Pérez-Fígares, J. M., & Rodríguez, E. M. (2005). Ependymal denudation and alterations of the subventricular zone occur in human fetuses with a moderate communicating hydrocephalus. *Journal of Neuropathology & Experimental Neurology*, 64(7), 595-604.

- Dosenbach, N. U., Fair, D. A., Miezin, F. M., Cohen, A. L., Wenger, K. K., Dosenbach, R. A., ... & Schlaggar, B. L. (2007). Distinct brain networks for adaptive and stable task control in humans. *Proceedings of the National Academy of Sciences*, *104*(26), 11073-11078.
- Dupont, P., Orban, G. A., De Bruyn, B., Verbruggen, A., & Mortelmans, L. (1994). Many areas in the human brain respond to visual motion. *Journal of neurophysiology*, *72*(3), 1420-1424.
- Egnor, M., Zheng, L., Rosiello, A., Gutman, F., & Davis, R. (2002). A model of pulsations in communicating hydrocephalus. *Pediatric neurosurgery*, *36*(6), 281-303.
- Erickson, K., Baron, I. S., & Fantie, B. D. (2001). Neuropsychological functioning in early hydrocephalus: Review from a developmental perspective. *Child Neuropsychology*, *7*(4), 199-229.
- Fletcher, J. M., Brookshire, B. L., Landry, S. H., Bohan, T. P., Davidson, K. C., Francis, D. J., ... & Morris, R. D. (1996). Attentional skills and executive functions in children with early hydrocephalus. *Developmental Neuropsychology*, *12*(1), 53-76.
- Fletcher, J. M., Dennis, M., & Northrup, H. (2000). Hydrocephalus.
- Fletcher, J. M., Francis, D. J., Thompson, N. M., Brookshire, B. L., Bohan, T. P., Landry, S. H., ... & Miner, M. E. (1992). Verbal and nonverbal skill discrepancies in hydrocephalic children. *Journal of Clinical and Experimental Neuropsychology*, *14*(4), 593-609.
- Fletcher, J. M., McCauley, S. R., Brandt, M. E., Bohan, T. P., Kramer, L. A., Francis, D. J., ... & Brookshire, B. L. (1996). Regional brain tissue composition in children with hydrocephalus: Relationships with cognitive development. *Archives of Neurology*, *53*(6), 549-557.
- Fonov, V., Evans, A. C., Botteron, K., Almli, C. R., McKinstry, R. C., Collins, D. L., & Brain Development Cooperative Group. (2011). Unbiased average age-appropriate atlases for pediatric studies. *Neuroimage*, *54*(1), 313-327.

- Fonov, V. S., Evans, A. C., McKinstry, R. C., Almlil, C. R., & Collins, D. L. (2009). Unbiased nonlinear average age-appropriate brain templates from birth to adulthood. *NeuroImage*, (47), S102.
- Gioia, G.A., Isquith, P.K., Guy, S.C., & Kenworthy, L. (2000). Behavior Rating Inventory of Executive Function. Odessa, FL: Psychological Assessment Resources.
- Girard, G., Whittingstall, K., Deriche, R., & Descoteaux, M. (2014). Towards quantitative connectivity analysis: reducing tractography biases. *Neuroimage*, 98, 266-278.
- Gmeiner, M., Wagner, H., Schlögl, C., van Ouwerkerk, W. J., Senker, W., Sardi, G., ... & Gruber, A. (2019). Adult Outcome in Shunted Pediatric Hydrocephalus: Long-Term Functional, Social, and Neurocognitive Results. *World neurosurgery*, 132, e314-e323.
- Gorgolewski, K. J., Auer, T., Calhoun, V. D., Craddock, R. C., Das, S., Duff, E. P., ... & Handwerker, D. A. (2016). The brain imaging data structure, a format for organizing and describing outputs of neuroimaging experiments. *Scientific data*, 3(1), 1-9.
- Götz, M., & Huttner, W. B. (2005). The cell biology of neurogenesis. *Nature reviews Molecular cell biology*, 6(10), 777-788.
- Greene, D. J., Koller, J. M., Hampton, J. M., Wesevich, V., Van, A. N., Nguyen, A. L., ... & Shimony, J. S. (2018). Behavioral interventions for reducing head motion during MRI scans in children. *NeuroImage*, 171, 234-245.
- Greene, R. (2014). *Attention and Executive Functioning in Patients With Hydrocephalus: A Meta-Analysis*. Wheaton College.
- Haber S. N. (2016). Corticostriatal circuitry. *Dialogues in clinical neuroscience*, 18(1), 7–21.
- Hagmann, P., Cammoun, L., Gigandet, X., Meuli, R., Honey, C. J., Wedeen, V. J., & Sporns, O. (2008). Mapping the structural core of human cerebral cortex. *PLoS biology*, 6(7).
- Hähnel, S., Freund, M., Münkler, K., Heiland, S., Jansen, O., Reidel, M., & Sartor, K. (2000). Magnetisation transfer ratio is low in normal-appearing cerebral white matter in patients with normal pressure hydrocephalus. *Neuroradiology*, 42(3), 174-179.

- Hähnel, S., Münkler, K., Jansen, O., Heiland, S., Reidel, M., Freund, M., ... & Sartor, K. (1999). Magnetization transfer measurements in normal-appearing cerebral white matter in patients with chronic obstructive hydrocephalus. *Journal of computer assisted tomography*, 23(4), 516-520.
- Hannay, H. J. (2000). Functioning of the corpus callosum in children with early hydrocephalus. *Journal of the International Neuropsychological Society*, 6(3), 351-361.
- Hashi, Ikhlas Ahmed, "Neurodevelopmental Outcomes of Infantile Hydrocephalus: An fMRI Case Study" (2019). Electronic Thesis and Dissertation Repository. 6313.
<https://ir.lib.uwo.ca/etd/6313>
- Hetherington, R., Dennis, M., Barnes, M., Drake, J., & Gentili, F. (2006). Functional outcome in young adults with spina bifida and hydrocephalus. *Child's Nervous System*, 22(2), 117-124.
- Hirsch, J. F. (1992). Surgery of hydrocephalus: past, present and future. *Acta neurochirurgica*, 116(2-4), 155-160.
- Hydrocephalus (2020). Wikipedia. Available at:
<https://en.wikipedia.org/w/index.php?title=Hydrocephalus&oldid=881990572> [Accessed May 20, 2020].
- Iloff, J. J., Wang, M., Liao, Y., Plogg, B. A., Peng, W., Gundersen, G. A., ... & Nagelhus, E. A. (2012). A paravascular pathway facilitates CSF flow through the brain parenchyma and the clearance of interstitial solutes, including amyloid β . *Science translational medicine*, 4(147), 147ra111-147ra111.
- Isaacs, A. M., Smyser, C. D., Lean, R. E., Alexopoulos, D., Han, R. H., Neil, J. J., ... & Limbrick Jr, D. D. (2019). MR diffusion changes in the perimeter of the lateral ventricles demonstrate periventricular injury in post-hemorrhagic hydrocephalus of prematurity. *NeuroImage: Clinical*, 24, 102031.
- Kahle, K. T., Kulkarni, A. V., Limbrick Jr, D. D., & Warf, B. C. (2016). Hydrocephalus in children. *The lancet*, 387(10020), 788-799.

- Kahle, K. T., Kulkarni, A. V., Limbrick Jr, D. D., & Warf, B. C. (2016). Hydrocephalus in children. *The lancet*, 387(10020), 788-799.
- Kestle, J. R., Riva-Cambrin, J., Wellons, J. C., Kulkarni, A. V., Whitehead, W. E., Walker, M. L., ... & Holubkov, R. (2011). A standardized protocol to reduce cerebrospinal fluid shunt infection: the Hydrocephalus Clinical Research Network Quality Improvement Initiative. *Journal of Neurosurgery: Pediatrics*, 8(1), 22-29.
- Kishimoto, J., Fenster, A., Lee, D. S., & de Ribaupierre, S. (2018). Quantitative 3-D head ultrasound measurements of ventricle volume to determine thresholds for preterm neonates requiring interventional therapies following posthemorrhagic ventricle dilatation. *Journal of Medical Imaging*, 5(2), 026001.
- Klingberg, T., Vaidya, C. J., Gabrieli, J. D., Moseley, M. E., & Hedehus, M. (1999). Myelination and organization of the frontal white matter in children: a diffusion tensor MRI study. *Neuroreport*, 10(13), 2817-2821.
- Krueger Jr, R. C. (2004). Use of a novel double-sandwich enzyme-linked immunosorbent assay method for assaying chondroitin sulfate proteoglycans that bear 3-nitrotyrosine core protein modifications, a previously unrecognized proteoglycan modification in hydrocephalus. *Analytical biochemistry*, 325(1), 52-61.
- Kulkarni, A. V., Riva-Cambrin, J., Butler, J., Browd, S. R., Drake, J. M., Holubkov, R., ... & Wellons, J. C. (2013). Outcomes of CSF shunting in children: comparison of Hydrocephalus Clinical Research Network cohort with historical controls. *Journal of Neurosurgery: Pediatrics*, 12(4), 334-338.
- Lehtinen, M. K., Bjornsson, C. S., Dymecki, S. M., Gilbertson, R. J., Holtzman, D. M., & Monuki, E. S. (2013). The choroid plexus and cerebrospinal fluid: emerging roles in development, disease, and therapy. *Journal of Neuroscience*, 33(45), 17553-17559.
- Lehtinen, M. K., Zappaterra, M. W., Chen, X., Yang, Y. J., Hill, A. D., Lun, M., ... & D'Ercole, A. J. (2011). The cerebrospinal fluid provides a proliferative niche for neural progenitor cells. *Neuron*, 69(5), 893-905.

- Lester, B. D., & Dassonville, P. (2014). The role of the right superior parietal lobule in processing visual context for the establishment of the egocentric reference frame. *Journal of Cognitive Neuroscience*, 26(10), 2201-2209.
- Ludwin, S. K. (1980). Chronic demyelination inhibits remyelination in the central nervous system. An analysis of contributing factors. *Laboratory investigation; a journal of technical methods and pathology*, 43(4), 382-387.
- Mahone, E. M., Zabel, T. A., Levey, E., Verda, M., & Kinsman, S. (2002). Parent and self-report ratings of executive function in adolescents with myelomeningocele and hydrocephalus. *Child Neuropsychology*, 8(4), 258-270.
- Mahone, E.M., Cirino, P., Cutting, L.E., Cerrone, P.M., Hagelthorn, K.M., Hiemenz, J.H., Singer, H.S., & Denckla, M.B. (2002). Validity of the Behavior Rating Inventory of Executive Function in children with ADHD and/or Tourette syndrome. *Archives of Clinical Neuropsychology*, 17(7), 643–662.
- Mangano, F. T., Altaye, M., McKinstry, R. C., Shimony, J. S., Powell, S. K., Phillips, J. M., Barnard, H., Limbrick, D. D., Jr, Holland, S. K., Jones, B. V., Dodd, J., Simpson, S., Mercer, D., Rajagopal, A., Bidwell, S., & Yuan, W. (2016). Diffusion tensor imaging study of pediatric patients with congenital hydrocephalus: 1-year postsurgical outcomes. *Journal of neurosurgery. Pediatrics*, 18(3), 306–319.
- Marek, S., Tervo-Clemmens, B., Nielsen, A. N., Wheelock, M. D., Miller, R. L., Laumann, T. O., ... & Perrone, A. (2019). Identifying reproducible individual differences in childhood functional brain networks: An ABCD study. *Developmental cognitive neuroscience*, 40, 100706.
- Mataró, M., Junqué, C., Poca, M. A., & Sahuquillo, J. (2001). Neuropsychological findings in congenital and acquired childhood hydrocephalus. *Neuropsychology review*, 11(4), 169-178.
- Perry, A., Wen, W., Lord, A., Thalamuthu, A., Roberts, G., Mitchell, P. B., ... & Breakspear, M. (2015). The organisation of the elderly connectome. *Neuroimage*, 114, 414-426.

- Petrides, M. (2005). Lateral prefrontal cortex: architectonic and functional organization. *Philosophical Transactions of the Royal Society B: Biological Sciences*, 360(1456), 781-795.
- Pettorossi, V. E., Di Rocco, C., Mancinelli, R., Caldarelli, M., & Velardi, F. (1978). Communicating hydrocephalus induced by mechanically increased amplitude of the intraventricular cerebrospinal fluid pulse pressure: rationale and method. *Experimental neurology*, 59(1), 30-39.
- Qiu, W., Chen, Y., Kishimoto, J., De Ribaupierre, S., Chiu, B., Fenster, A., ... & Yuan, J. (2016). Longitudinal analysis of pre-term neonatal cerebral ventricles from 3D ultrasound images using spatial-temporal deformable registration. *IEEE transactions on medical imaging*, 36(4), 1016-1026.
- Rekate, H. L. (2008). The definition and classification of hydrocephalus: a personal recommendation to stimulate debate. *Cerebrospinal fluid research*, 5(1), 2.
- Renier, L. A., Anurova, I., De Volder, A. G., Carlson, S., VanMeter, J., & Rauschecker, J. P. (2010). Preserved functional specialization for spatial processing in the middle occipital gyrus of the early blind. *Neuron*, 68(1), 138-148.
- Reynolds, C.R., & Kamphaus, R.W. (1998a). Behavior Assessment System for Children. Parent Rating Scale. Circle Pines, MN: *American Guidance Services*.
- Reynolds, C.R., & Kamphaus, R.W. (1998b). Behavior Assessment System for Children. Self-Report Version. Circle Pines, MN: *American Guidance Services*
- Roberts, J. A., Perry, A., Roberts, G., Mitchell, P. B., & Breakspear, M. (2017). Consistency-based thresholding of the human connectome. *Neuroimage*, 145, 118-129.
- Robertson, B. D., Hiebert, N. M., Seergobin, K. N., Owen, A. M., & MacDonald, P. A. (2015). Dorsal striatum mediates cognitive control, not cognitive effort per se, in decision-making: An event-related fMRI study. *Neuroimage*, 114, 170-184.

- Rubinov, M., & Sporns, O. (2010). Complex network measures of brain connectivity: uses and interpretations. *Neuroimage*, 52(3), 1059-1069.
- Sakka, L., Coll, G., & Chazal, J. (2011). Anatomy and physiology of cerebrospinal fluid. *European annals of otorhinolaryngology, head and neck diseases*, 128(6), 309-316.
- Scheel, M., Diekhoff, T., Sprung, C., & Hoffmann, K. T. (2012). Diffusion tensor imaging in hydrocephalus—findings before and after shunt surgery. *Acta neurochirurgica*, 154(9), 1699-1706.
- Schurz, M., Aichhorn, M., Martin, A., & Perner, J. (2013). Common brain areas engaged in false belief reasoning and visual perspective taking: a meta-analysis of functional brain imaging studies. *Frontiers in human neuroscience*, 7, 712.
- Shang, C. Y., Wu, Y. H., Gau, S. S., & Tseng, W. Y. (2013). Disturbed microstructural integrity of the frontostriatal fiber pathways and executive dysfunction in children with attention deficit hyperactivity disorder. *Psychological medicine*, 43(5), 1093-1107.
- Shulman, G. L., Schwarz, J., Miezin, F. M., & Petersen, S. E. (1998). Effect of motion contrast on human cortical responses to moving stimuli. *Journal of neurophysiology*, 79(5), 2794-2803
- Smith, S., Bannister, P. R., Beckmann, C., Brady, M., Clare, S., Flitney, D., ... & Woolrich, M. (2001). FSL: New tools for functional and structural brain image analysis. *NeuroImage*, 13(6), 249.
- Smyser, C. D., Snyder, A. Z., Shimony, J. S., Blazey, T. M., Inder, T. E., & Neil, J. J. (2013). Effects of white matter injury on resting state fMRI measures in prematurely born infants. *PloS one*, 8(7).
- Smyser, C. D., Wheelock, M. D., Limbrick Jr, D. D., & Neil, J. J. (2019). Neonatal brain injury and aberrant connectivity. *NeuroImage*, 185, 609-623.

- Socci, D. J., Bjugstad, K. B., Jones, H. C., Pattisapu, J. V., & Arendash, G. W. (1999). Evidence that oxidative stress is associated with the pathophysiology of inherited hydrocephalus in the H-Tx rat model. *Experimental neurology*, *155*(1), 109-117.
- Song, S. K., Yoshino, J., Le, T. Q., Lin, S. J., Sun, S. W., Cross, A. H., & Armstrong, R. C. (2005). Demyelination increases radial diffusivity in corpus callosum of mouse brain. *Neuroimage*, *26*(1), 132-140.
- Swanson, J., Castellanos, F. X., Murias, M., LaHoste, G., & Kennedy, J. (1998). Cognitive neuroscience of attention deficit hyperactivity disorder and hyperkinetic disorder. *Current opinion in neurobiology*, *8*(2), 263-271.
- Tanaka, E., Inui, K., Kida, T., & Kakigi, R. (2009). Common cortical responses evoked by appearance, disappearance and change of the human face. *BMC neuroscience*, *10*(1), 38.
- Tibshirani, R. J., & Efron, B. (1993). An introduction to the bootstrap. *Monographs on statistics and applied probability*, *57*, 1-436.
- Toga, A. W., Thompson, P. M., & Sowell, E. R. (2006). Mapping brain maturation. *Focus*, *29*(3), 148-390.
- Tu, S., Qiu, J., Martens, U., & Zhang, Q. (2013). Category-selective attention modulates unconscious processes in the middle occipital gyrus. *Consciousness and Cognition*, *22*(2), 479-485.
- Tziortzi, A. C., Haber, S. N., Searle, G. E., Tsoumpas, C., Long, C. J., Shotbolt, P., ... & Jenkinson, M. (2014). Connectivity-based functional analysis of dopamine release in the striatum using diffusion-weighted MRI and positron emission tomography. *Cerebral Cortex*, *24*(5), 1165-1177.
- Veening, J. G., & Barendregt, H. P. (2010). The regulation of brain states by neuroactive substances distributed via the cerebrospinal fluid; a review. *Cerebrospinal Fluid Research*, *7*(1), 1.

- Wagshul, M. E., Eide, P. K., & Madsen, J. R. (2011). The pulsating brain: a review of experimental and clinical studies of intracranial pulsatility. *Fluids and Barriers of the CNS*, 8(1), 5.
- Wilkinson, L. (1999). Statistical methods in psychology journals: Guidelines and explanations. *American psychologist*, 54(8), 594.
- Wright, D. B. (2003). Making friends with your data: Improving how statistics are conducted and reported. *British Journal of Educational Psychology*, 73, 123–136.
- Yuan, W., Deren, K. E., McAllister, J. P., Holland, S. K., Lindquist, D. M., Cancelliere, A., ... & Mangano, F. T. (2010). Diffusion tensor imaging correlates with cytopathology in a rat model of neonatal hydrocephalus. *Cerebrospinal fluid research*, 7(1), 19.
- Yuan, W., Holland, S. K., Shimony, J. S., Altaye, M., Mangano, F. T., Limbrick, D. D., ... & Ragan, D. (2015). Abnormal structural connectivity in the brain networks of children with hydrocephalus. *NeuroImage: Clinical*, 8, 483-492.
- Yuan, W., Meller, A., Shimony, J. S., Nash, T., Jones, B. V., Holland, S. K., ... & McKinstry, R. C. (2016). Left hemisphere structural connectivity abnormality in pediatric hydrocephalus patients following surgery. *NeuroImage: Clinical*, 12, 631-639.
- Zaaraoui, W., Deloire, M., Merle, M., Girard, C., Raffard, G., Biran, M., ... & Franconi, J. M. (2008). Monitoring demyelination and remyelination by magnetization transfer imaging in the mouse brain at 9.4 T. *Magnetic Resonance Materials in Physics, Biology and Medicine*, 21(5), 357-362.

Appendix A



Date: 4 April 2019

To: Sandrine de Ribaupierre

Project ID: 104107

Study Title: Brain variability in children with previous IVH - a pilot study

Application Type: HSREB Amendment Form

Review Type: Delegated

Full Board Reporting Date: April 23, 2019

Date Approval Issued: 04/Apr/2019

REB Approval Expiry Date: 30/Jan/2020

Dear Sandrine de Ribaupierre ,

The Western University Health Sciences Research Ethics Board (HSREB) has reviewed and approved the WREM application form for the amendment, as of the date noted above.

Documents Approved:

Document Name	Document Type	Document Date
104107protocol_Changes_April2019	Protocol	Received April 1, 2019
BRIEF2	Paper Survey	Received April 1, 2019
Brochure_hydrocephalus	Recruitment Materials	Received April 1, 2019
Email_phone_Script	Recruitment Materials	Received April 1, 2019
poster_hydrocephalus	Recruitment Materials	Received April 1, 2019
REB_Brain_Variability_IVH_LOC_control_April	Consent Form	01/Apr/2019
REB_Brain_Variability_IVH_LOC_patient_April	Consent Form	01/Apr/2019
SES	Online Survey	Received April 1, 2019
SES	Paper Survey	Received April 1, 2019

REB members involved in the research project do not participate in the review, discussion or decision.

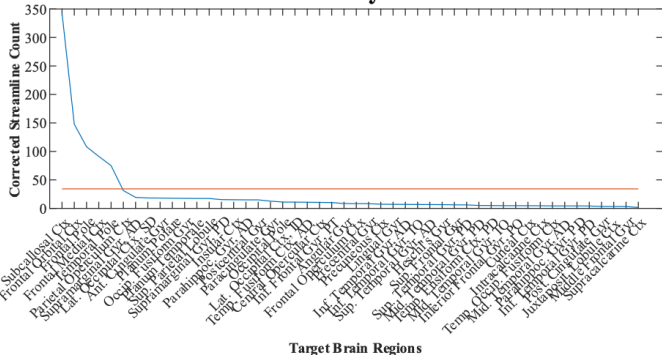
The Western University HSREB operates in compliance with, and is constituted in accordance with, the requirements of the TriCouncil Policy Statement: Ethical Conduct for Research Involving Humans (TCPS 2); the International Conference on Harmonisation Good Clinical Practice Consolidated Guideline (ICH GCP); Part C, Division 5 of the Food and Drug Regulations; Part 4 of the Natural Health Products Regulations; Part 3 of the Medical Devices Regulations and the provisions of the Ontario Personal Health Information Protection Act (PHIPA 2004) and its applicable regulations. The HSREB is registered with the U.S. Department of Health & Human Services under the IRB registration number IRB 00000940.

Please do not hesitate to contact us if you have any questions.

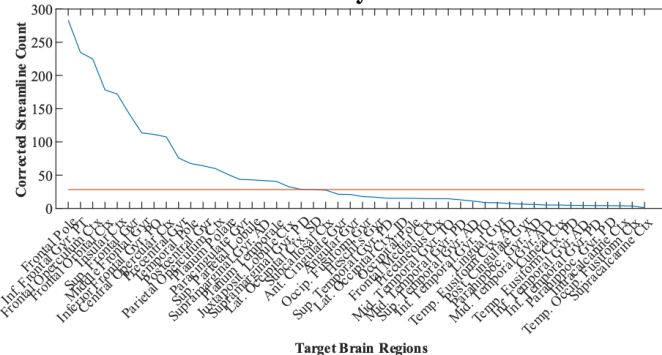
Appendix A: Research Ethics Board Approval

Appendix B

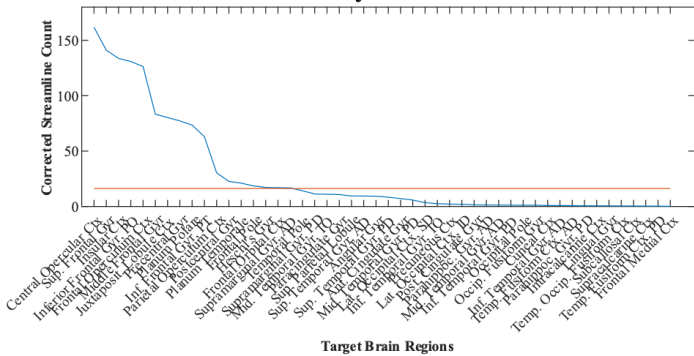
Rank-ordered Connectivity of the Striatum limbic



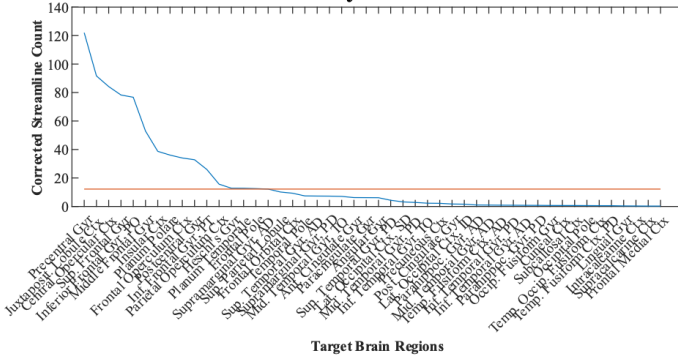
Rank-ordered Connectivity of the Striatum Executive



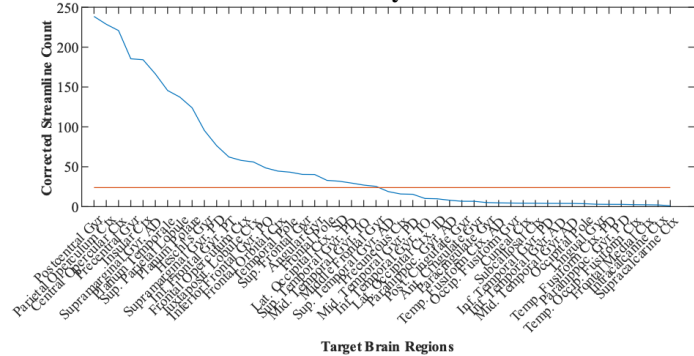
Rank-ordered Connectivity of the Striatum Rostral-Motor



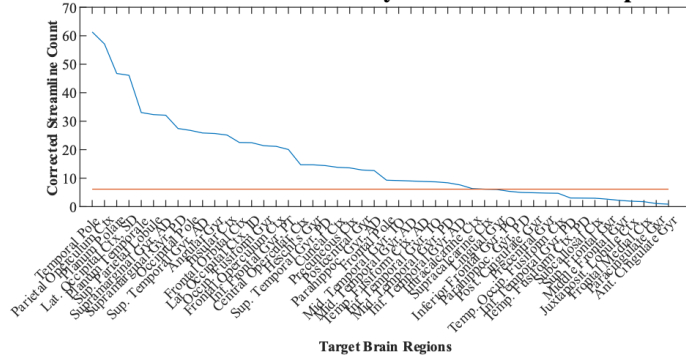
Rank-ordered Connectivity of the Striatum Caudal-Motor



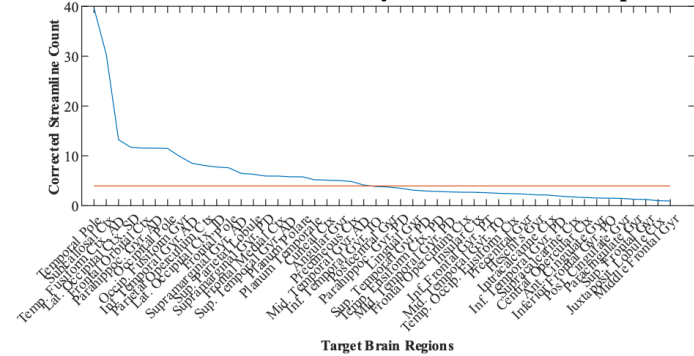
Rank-ordered Connectivity of the Striatum Parietal



Rank-ordered Connectivity of the Striatum Occipital



Rank-ordered Connectivity of the Striatum Temporal



Appendix B: Threshold for striatal networks

Curriculum Vitae

Name:	Daamoon Ghahari
Post-secondary Education and Degrees:	Western University London, Ontario, Canada 2013-2018 BSc. Honours Specialization in Neuroscience Major in Genetics
	Western University London, Ontario, Canada 2018-2020 MSc. Candidate Neuroscience
Honours and Awards:	Natural Sciences and Engineering Research Council (NSERC-USRA) 2018
	Natural Sciences and Engineering Research Council (NSERC- CGS-M) 2019-2020
Related Work Experience	Teaching Assistant Western University 2018-2020
	Undergraduate Research Assistant 2013-2018
	Graduate Research Assistant 2018-2020

Publications and Conference Presentations

- Ghahari, Daamoon**, Individual Differences in Impulsivity and Mesocorticolimbic Connectivity Strength in Pre-adolescence (2018). 2018 Undergraduate Awards. 16. https://ir.lib.uwo.ca/undergradawards_2018/16
- Ghahari, Daamoon**, The Effects of Lipopolysaccharide on Positive Reinforcement in Rats" (2018). 2018 Undergraduate Awards. 15. https://ir.lib.uwo.ca/undergradawards_2018/15

Ghahari, D., Hashi, I, A., Morton, J, B., Eagleson, R. & de Ribaupierre, S. (2019, May). Executive dysfunction and white matter integrity in children with hydrocephalus years after surgery. Abstract accepted to the Southern Ontario Neuroscience Association Annual Meeting, Windsor, ON.

Daamoon Ghahari, Roy Eagleson, J Bruce Morton, and Sandrine de Ribaupierre. (2020, June). Altered Probabilistic Connectivity of Striatal-Executive Networks in Children with Hydrocephalus. Abstract accepted to Organization for Human Brain Mapping (OHBM), Online, June 23rd 2020.